DELIVERABLE D3.2

INTEGRATION AND TESTING RESULTS AND PERFORMANCE ANALYSIS

JANUARY 15, 2024

MARIOS RASPOPOULOS, STELIOS IOANNOU, ANDREY SESYUK

INTERDISCIPLINARY SCIENCE PROMOTION & INNOVATIVE RESEARCH EXPLORATION (INSPIRE)

Co-funded by the European Union

Republic of Cyprus

RESEARCH & INNOVATION FOUNDATION

"This work was co-funded by the European Union under the programme of social cohesion "THALIA 2021-2027", through Research and Innovation Foundation (Project: CONCEPT/0722/0031)".

Abstract

This report describes and evaluates the results of the performance of the various positioning algorithms tested using the proposed technology and discusses the challenges faced and how they were overcome.

It presents the results and performance analysis of the proposed methods for single target positioning and multitarget positioning and compares the results against results reported in literature. This reports constitutes the asssement of quality of the project output and in order to make the discussion complete some results and or descriptions provided in deliverables D4.1 and D4.2 are presented here as well. Over all the THESIS project has managed to achieve the objective of achieving decimeter-level accuracy for single-target (~15cm) and multi-target (~25cm) scenaria. Different approaches have been used which are discussed in detail in this report.

The project team has managed to publish two papers within the scope of this project:

A. Sesyuk, S. Ioannou and M. Raspopoulos, "3D millimeter-Wave Indoor Localization," *2023 13th International Conference on Indoor Positioning and Indoor Navigation (IPIN)*, Nuremberg, Germany, 2023, pp. 1-7, doi: 10.1109/IPIN57070.2023.10332537.
B. Sesyuk, S. Ioannou and M. Raspopoulos, " Radar-based millimeter-Wave sensing for accurate 3D Indoor Positioning - Potentials and Challenges," *IEEE Journal Of Indoor And Seamless Positioning And Navigation*, 2024, [ACCEPTED – in press].

The project team evaluates the performance and results of the proposed methodologies as excellent and that the project objectives have been met in full.

Table of Contents

1 Introduction

The explosive growth of the Internet of Things (IoT) and the emergence of many Location-Based Services (LBS) and mobile smart applications make localization an even more important key-enabling technology in the Information and Communications Technology (ICT) world while many of these LBSs impose very high 3D localization accuracy requirements. Several approaches have been proposed during the last few decades to address the challenges of indoor localization however most of them only estimate positions on a horizontal *(x-y)* plane and many times neglect the vertical *(z)* dimension. This lack of vertical information could lead into problems, such as the inability to determine whether a device is held up high or in a pocket etc., while accurate 3D positioning is also critical in scenarios such as drone-assisted crop seeding, search and rescue operations, and wireless communication (Han C. &., 2012), where sub-meter or cm-level accuracy is likely essential.

To address this demand, millimeter-wave (mmWave) positioning systems have emerged as a promising technology, offering high accuracy and robustness. mmWave is currently used in some Wi-Fi systems (e.g. IEEE802.11ad) while it is planned to be used in 5G communications due to its flexibility to use wider bandwidths and hence its strong potential in achieving much higher data rates and capacity. mmWave systems typically operate in frequencies between 26 to 100*GHz*. At those very high frequencies there is large availability of bandwidth which could lead to fine timing resolution and hence high ranging accuracy. The very small wavelength also allows the development of small and compact massive phase antenna arrays that enable the accurate estimation of angles (azimuth and elevation) of arrival. All this accurate context could be used for achieving cm-level 3D positioning accuracy or better (D. Wang, 2019). In this work, we capitalize on the potential of mmWave technology to accurately provide ranging and angling information, and sustain the momentum of ongoing research efforts in this topic by demonstrating its suitability to achieve cm-level accuracy, while presenting the most important challenges it imposes.

In response to the increasing demand for precise 3D indoor positioning in smart applications, there has been a growing surge in research and development efforts in recent years. These efforts are aimed at exploring advanced technologies to meet this need. The authors of (A. Sesyuk S. I., A survey of 3d indoor localization systems and technologies, 2022) offer a comprehensive survey of 3D indoor localization techniques and approaches. It delves into various modern technologies, providing insights and evaluations. Notably, the authors of this paper reference some relevant works. For example, in (A. Shahmansoori, 2018), the authors theoretically derive the Cramér-Rao Bound (CRB) for position and rotation angle estimation uncertainty using mmWave signals from a single transmitter, even in the presence of scatterers. They demonstrate that under open Line of Sight (LoS) conditions, it is feasible to estimate a target's position and orientation angle by leveraging information from multipath signals. However, this approach comes with a noticeable performance penalty. Additionally, the authors of (Y. Han, 2016) showcase the advantages of array antennas in

determining a device's orientation. Notably, the accuracy of mmWave technology-based positioning appears to be closely linked to the distance from the target. In a study mentioned in (Ojas Kanhere, 2018), the authors conduct Angle of Arrival (AoA) and signal measurements in a 35*m* x 65.5*m* open space, achieving position accuracy ranging from 16*cm* to 3.25*m*. While positioning research using this mmWave technology is in its early stages, early theoretical findings and practical experiments reveal its potential to deliver the high accuracy demanded by modern smart applications. In a different context, (Hao, et al., 2022) introduces a multipath-assisted localization (MAL) model based on mmWave radar for indoor electronic device localization. This model effectively incorporates multipath effects when describing reflected signals, enabling precise target position determination using the MAL area formed by the reflected signal. Importantly, this model can provide 3D target information even when traditional Single-Input Single-Output (SISO) radar falls short. Furthermore, in a scenario described in (Y. Jia, 2018), an indoor office setting with a single mmWave base station (BS) is considered. The authors propose a method that fuses user equipment (UE) motion features, mmWave line-of-sight (LoS), and first-order reflection paths' Angle of Arrival (AoA) and Time of Arrival (ToA) for indoor positioning. They present an improved least mean square (LMS) algorithm to refine multipath AoA estimation and a modified multipath unscented Kalman filter (UKF) for position tracking. The results of these methods show significant enhancements in LoS-AoA estimation and centimeter-level 3D positioning accuracy, around 60*cm*. Notably, this strategy is effective even in scenarios with insufficient anchor nodes. In an alternative approach, as presented in (Youqing Wang, 22), a method for achieving 3D indoor positioning using a single base station is proposed. This approach leverages multipath channels, with MIMO antennas estimating the angles of multipath coherent signals, and OFDM signals handling delay estimation. By integrating MIMO and OFDM technologies within a wireless communication system, an array antenna is employed to estimate the AoA of multipath signals. Spatial smoothing algorithms are applied in the frequency domain to estimate the Time Difference of Arrival (TDoA) of multiple coherent signals. This approach has been validated through simulations in a 6*m* x 8*m* x 4.5*m* indoor space. The results indicate that positioning accuracy reaches submeter levels in 95% of cases and is less than 0.4*m* in 60% of cases. The authors of (Z. Lin, 2018), present a novel 3-D indoor positioning scheme using mmWave massive multiple-input multiple-output (mMIMO) systems. The operation of this scheme is based on a hybrid received signal strength and angle of arrival (RSS-AoA) positioning scheme, which employs only a single access point equipped with a large-scale uniform cylindrical array. The authors design a novel hybrid RSS-AoA positioning scheme for the computations of the 3-D coordinates of the target mobile terminal. They demonstrate that their approach achieves azimuth and elevation precision around 0.5 degrees depending on the quality of the received signal. In (Tuo Wu, 2022), the authors investigate a 3D positioning algorithm for a mmWave system leveraging Reconfigurable Intelligent Surfaces (RIS) to enhance the positioning performance of mobile users (MUs). They use a two-stage weight least square (TSWLS) algorithm to obtain the closed-form solution of the MU's position. Similarly in (Yin, 2021), the authors address the channel estimation for RIS-aided mmWave communication systems based on a localization method. They propose the concept of reflecting unit set (RUS) to improve the flexibility of RIS. The authors then propose a novel

coplanar maximum likelihood-based (CML) 3D positioning method based on the RUS and derive the Cramer-Rao lower bound (CRLB) for the positioning method. Furthermore, they develop an efficient positioning-based channel estimation scheme with low computational complexity. They demonstrate that cm-level accuracy can be achieved averaging around 5*cm* depending on the received signal quality. A 60GHz signal-based positioning and tracking system is discussed in (A. Antonucci, 2019) , which effectively filters out multiple reflections and diffuse scattering, ensuring a high level of accuracy. Operating within a longitudinal range of 0.46m to 5.55m and a lateral span from 1.91m to 3.04m, the system determines the target's position through the calculation of the local centroid in the associated point cloud. Overall, the system achieves a plane positioning accuracy with a 99% confidence level and an error of approximately 30–40cm. In another work (Maisy Lam, 2023), the authors have presented a self-localization system for autonomous drones that utilizes a single millimeter-Wave anchor. The system leverages a novel dual polarized, dual modulated mmWave anchor and mmWave-IMU Fusion self-localization algorithm to ultimately achieve precise, high-speed 3D localization. The authors have demonstrated a median localization error of 7*cm* and a 90th percentile less than 15*cm*, even in NLOS scenarios. Another work positioning a drone is presented in (Hunukumbure, 2022) where the authors developed a 3GPP-compliant drone-based 3D indoor local- ization solution employing an integration of time-based and angle-based techniques to improve the situational awareness in emergency situations and support emergency services. They have managed to achieve a horizontal and vertical positional error 1.05m and 0.7m at 26GHz frequency. A similar work is presented in (F. Parralejo, 2023) where the authors propose a security system based on millimetre-wave radar, using a processing workflow based on machine learning techniques, achieving 99.32% accuracy and 99.54% F1 score. Another work utilizing machine learning is presented in (P. K. Rai, 2021), where a custom CNN model achieves an accuracy of 95%. (Marques, 2020) presents an active drone detection system that uses a millimeter wave radar mounted on a drone to estimate 3D position of the target drone using 2D measurements. The results indicated an average 3D positioning error of 2.17m.

2 Results

2.1 2-DOF Setup Results

Utilizing the experimental setup described in Deliverable D4.1, a set of ranging and angular measurements was collected from TI mmWave sensors while the drone was flown at 8 well-known 3D locations as shown in Figure 1. Using these measurements 3D positioning estimation was conducted both using a two 3D multilateration and a triangulation approach. Ground-truth location precision is crucial for the validity of this work as it serves as the reference for evaluating the accuracy of the approach. While flying around the lab, the drone was instructed to hover at the particular points of interest and while hovering the precise location of the drone was determined using a laser distance measuring tool. Essentially, the laser tool was secured using a tripod at the location of the drone while the latter was hovering and

distance measurements were taken to the horizontal and vertical walls of the lab as well as to the floor determining the precise *x,y,z* location of the drone.

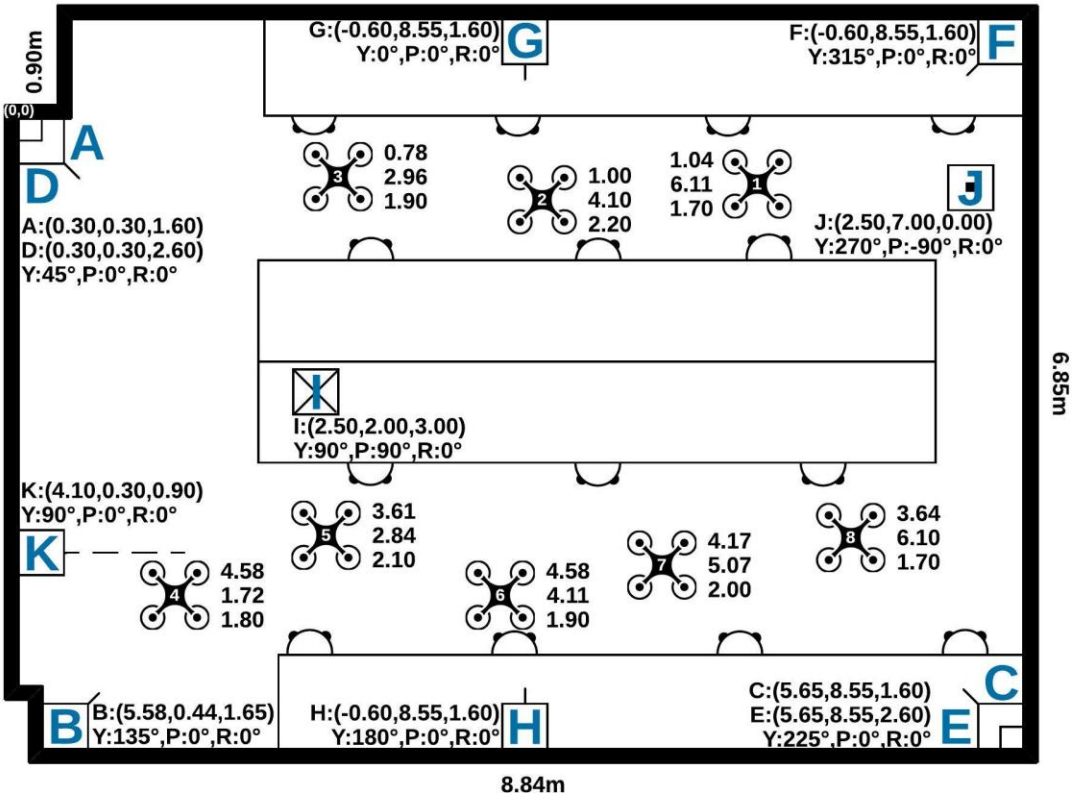

Figure 1 - mmWave 3D Positioning Experimental Setup using 2-DOF mmWave Sensors (Y: Yaw, P: Pitch, R: Roll)

2.1.1 3D Multilateration Approach

Multilateration serves as a fundamental technique for achieving 3D positioning across a wide range of scientific and technological domains. It harnesses distance measurements from multiple reference points to determine the exact location of an object within three-dimensional space by using at least 4 sensors. Through the exploitation of geometric relationships between the object and these reference points, multilateration algorithms facilitate the calculation of intersecting spheres or hyperboloids, ultimately yielding the object's coordinates. In this work, 3D position estimation is done using the standard algebraic solution (Malivert F, 2023) of the 3D multilateration problem as well as a recursive multilateration solution presented in (Norrdine, 2012). Different combinations of sensors were used to investigate the effects of DoP.

The first experiment was conducted using ranging measurements collected from 4 TI sensors deployed in the 4 corners of the room in locations **A,B,C** and **F** as shown in Figure 1 and the results for both the standard algebraic solution as well as the recursive one are tabulated in Table 1. It appears that an average error in the ranging measurement of 0.06*m* translates into a 0.14*m* and 0.1*m* average positioning error in *x* and *y* using the standard algebraic solution while a

considerable error is observed in the *z*-axis (5.72*m* average). These are translated into an average 3D positioning error of 5.76*m*. The results appear to improve when using the recursive multilateration approach (vertical error of 1.69*m* and an average 3D error of 1.72*m*), however the error in the vertical dimension still remains significant. This is attributed to the fact that all sensors are placed on the same height resulting in a very high Vertical Dilution of Precision (VDOP) averaging around 23.6.

Table 1 - 4 Anchor Configuration - Equal Height

Point	Distance Error *(m)*	Algebraic Solution				Recursive Solution				HDOP	VDOP
		Error XYZ *(m)*			3D Error *(m)*	Error XYZ *(m)*			3D Error *(m)*		
		x	*y*	*z*		*x*	*y*	*z*			
1	-0.04	0.12	0.23	0.08	0.27	0.02	-0.27	-1.02	1.05	1.12	43.05
2	-0.06	0.22	0.07	-9.46	9.46	0.28	-0.02	-1.23	1.26	1.10	25.95
3	0.09	0.12	0.00	-1.35	1.35	0.09	-0.12	0.36	0.39	1.11	4.95
4	0.03	-0.21	-0.09	0.43	0.49	-0.12	-0.22	4.77	4.78	1.11	8.35
5	-0.02	-0.22	0.12	-16.4	16.40	0.02	-0.26	2.39	2.40	1.06	4.95
6	0.10	-0.07	0.08	-11.1	11.11	0.00	-0.06	-1.68	1.68	1.11	10.59
7	-0.09	0.05	0.06	-6.56	6.56	0.39	0.09	1.54	1.59	1.24	44.70
8	-0.02	-0.13	-0.16	0.40	0.45	-0.22	0.17	-0.56	0.62	1.25	46.41
Average	***0.06***	***0.14***	***0.10***	***5.72***	***5.76***	***0.14***	***0.15***	***1.69***	***1.72***	***1.14***	***23.61***

Table 2 - 4 Anchor Configuration - Different Height

Point	Distance Error *(m)*	Algebraic Solution				Recursive Solution				HDOP	VDOP
		Error XYZ *(m)*			3D Error *(m)*	Error XYZ *(m)*			3D Error *(m)*		
		x	*y*	*z*		*x*	*y*	*z*			
1	0.07	-0.19	-0.20	-0.15	0.32	-0.29	0.00	-0.37	0.47	1.07	1.80
2	0.05	-0.09	-0.25	0.03	0.27	0.28	-0.31	-0.12	0.44	1.06	1.61
3	-0.14	0.23	0.02	0.47	0.52	0.11	-0.09	-0.33	0.36	1.12	1.75
4	-0.06	-0.13	-0.29	0.12	0.34	-1.59	-0.02	1.94	2.51	1.31	1.49
5	-0.06	0.08	0.02	-0.14	0.16	-2.94	-0.19	2.81	4.07	1.22	1.41
6	-0.12	0.21	0.07	0.03	0.22	-1.53	-0.27	1.96	2.50	1.07	1.03
7	0.13	0.06	-0.22	0.04	0.23	-0.39	-0.17	0.09	0.44	1.10	0.93
8	-0.07	-0.29	0.23	-0.11	0.38	0.13	0.27	-0.33	0.45	1.06	1.16
Average	***0.09***	***0.16***	***0.16***	***0.13***	***0.31***	***0.91***	***0.17***	***0.99***	***1.40***	***1.41***	***1.54***

Table 3 - 6 Anchor Configuration - Different Height

Point	Distance Error *(m)*	Algebraic Solution				Recursive Solution				HDOP	VDOP
		Error XYZ *(m)*			3D Error *(m)*	Error XYZ *(m)*			3D Error *(m)*		
		x	*y*	*z*		*x*	*y*	*z*			
1	0.00	-0.18	0.07	-0.56	0.59	-0.07	0.01	-0.14	0.15	0.93	1.60
2	-0.08	0.11	-0.05	-0.27	0.30	-0.12	-0.27	-0.06	0.30	0.95	1.63
3	0.04	-0.02	-0.03	0.17	0.17	0.64	0.01	0.67	0.93	0.93	1.70
4	-0.12	-0.04	0.11	-0.12	0.17	0.01	-0.34	-0.05	0.35	0.96	1.60
5	-0.02	-0.05	0.08	0.07	0.11	0.52	-0.15	0.03	0.55	0.93	1.44
6	-0.07	0.07	-0.03	0.07	0.10	-0.01	-0.14	-0.31	0.34	0.88	1.74
7	0.13	-0.08	-0.02	0.48	0.49	0.08	0.05	0.19	0.22	0.91	1.68
8	-0.11	0.03	0.00	-0.01	0.03	0.24	0.10	0.10	0.28	0.95	1.45
Average	***0.07***	***0.07***	***0.05***	***0.22***	***0.24***	***0.21***	***0.13***	***0.19***	***0.39***	***0.94***	***1.48***

DOP plays a crucial role in 3D indoor positioning, as it directly affects the accuracy and reliability of position estimates. While DOP values are commonly considered in the horizontal plane, they are equally important in the vertical plane (B. Li, 2020). Considering this, the reason why our results often exhibit better accuracy in the horizontal plane compared to the vertical plane can be attributed to the distribution of sensors. In the horizontal plane, the sensors are spread out more widely, allowing for better sensor geometry. This improved distribution of sensors results in lower HDOP values, indicating reduced potential for horizontal positioning errors. The IWR1642BOOST mmWave sensor, with its narrow 15-degree elevation field-of-view, poses a limitation on the distribution of sensors in the vertical plane. The narrower vertical perspective leads to a less favorable sensor geometry and higher VDOP values. As a consequence, the accuracy of height estimation in 3D positioning may be more susceptible to errors and uncertainties. Nevertheless, it was attempted to position 4 sensors at different heights ($1m$, $1.5m$, $2m$ and $2.5m$) to demonstrate the potential improvement. Table 2 verifies this hypothesis by indicating significant improvement of algebraic solution in the z-axis ($0.13m$) bringing the 3D positioning error down to $0.31m$ which is attributed to the significant improvement of the VDOP (average 1.54). Interestingly enough it appears that the recursive solution fails to identify the optimal solution leading to significantly high errors. To further investigate the DOP significance we set up another experiment consisting of 6 anchors (the four anchors of the previous case plus one sensor at the ceiling (position **I**) and one on the floor (position **J**). This new constellation or anchors reduces both the VDOP as well as the HDOP and this reflected on both the multilateration approches. The average 3D positioning error reduces down to $0.22m$ while the one from the recursive version reduces down to $0.39m$. Interestingly the standard algebraic solution still outperforms the recursive one as can be seen in Table 3.

2.1.2 3D Triangulation Approach

Considering the inaccuracy of the multilateration approach in the *z*-axis, particularly when DOP optimization is not possible, and capitalizing on the ability of the IWR1642BOOST sensor to measure the azimuth angle, the experimental setup was adjusted, deploying 2 sets of two sensors on top of each other as shown in Figure 3. Sensor D is placed on top of A, sensor E on top of C, while sensor F was left on its own on the far-most right corner. 3D position estimation is achieved by using a combination of typical triangulation formulation using the azimuth angles measured from the 3 corners while the *z*-axis coordinate is estimated based on the height formulation below which estimates the height *h* in the Complexity-Reduced Trilateration Approach (COLA) approach presented in (Marrón, 2010).

$$h = z_2 - \frac{d_2^2 - d_1^2 + (z_2 - z_1)^2}{2(z_2 - z_1)}$$

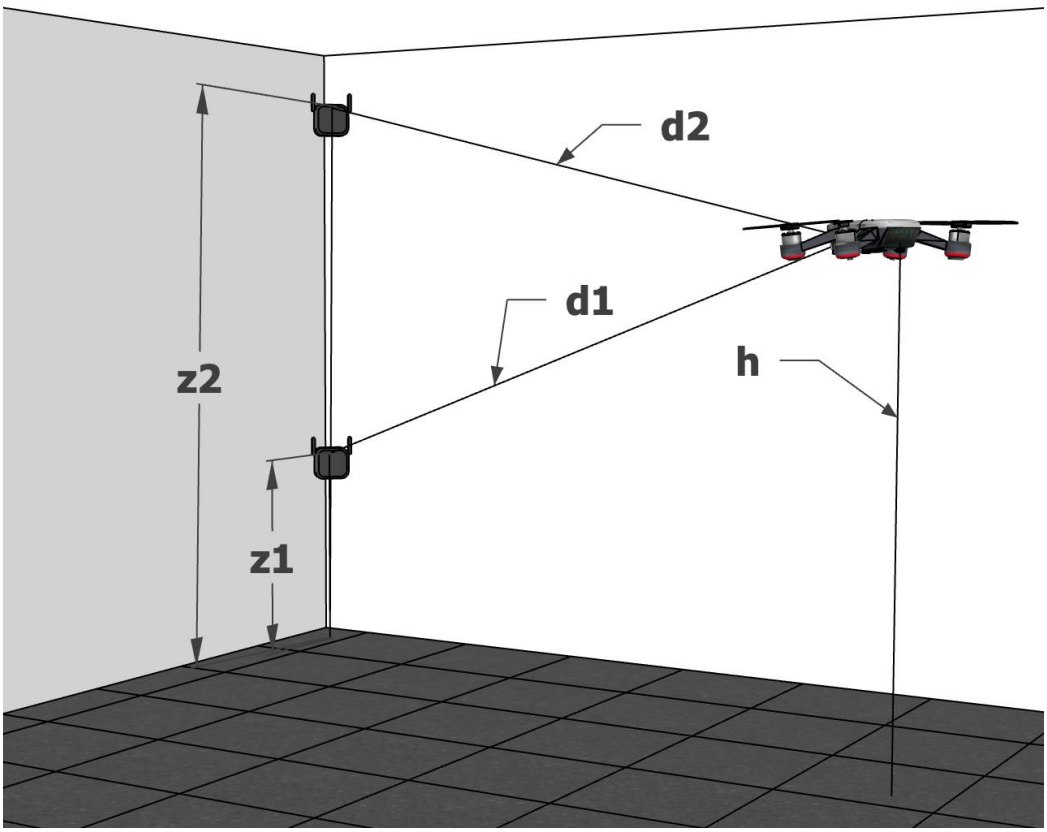

Figure 2 - 3D Triangulation - Sensor Arrangement

Results tabulated in Table 4 indicate a significant improvement in the *z*-axis (0.11*m*) while there is also a good improvement in the *x* and *y* axes (error being 0.09*m* and 0.08*m*) bringing the 3D positioning accuracy down to 0.17*m*.

Table 4 - 3D Triangulation Positioning

Point	Azimuth Error (°)	XYZ Error *(m)*			3D Error *(m)*
		x	*y*	*z*	
1	1.02	0.13	0.14	-0.03	0.20
2	0.72	-0.03	0.09	0.16	0.19
3	0.91	-0.08	-0.09	0.14	0.19
4	1.88	-0.04	-0.13	0.16	0.22
5	1.51	0.25	0.11	-0.13	0.31
6	0.91	0.09	-0.08	-0.30	0.32
7	0.39	0.06	0.03	0.04	0.08
8	2.20	0.05	-0.02	-0.03	0.06
Average	***1.20***	***0.09***	***0.08***	***0.11***	***0.17***

2.2 3-DOF Setup Results

Texas Instrument's IWR1843BOOST is considered as a newer upgrade to the IWR1642BOOST sensor used in the previous experiments. Due to an additional antenna, which provides the user with additional elevation data, allows for 3-DOF. This, in theory, means that it is worth capitalizing on the ability of the sensor to measure elevation in addition to azimuth and range to perform 3D positioning using a single anchor.

2.2.1 3-DOF Single Anchor 3D Positioning

To analyse the positioning accuracy when a single IWR1843BOOST sensor is used, a similar approach to that used in the precision analysis was adopted. This involved a drone flying in front of the sensor while the sensor was incrementally rotated to vary both azimuth and elevation angles. This experiment was conducted at various distances from the sensor to capture data across a range of positions.

Having available, the range (r), the azimuth (θ) and the elevation (φ) measurements from the anchor to the target one can estimate the coordinates of the target with respect to the body-frame coordinate system of the anchor using standard spherical to Cartesian coordinate conversion according to Figure 3 and Equation below:

$$\begin{bmatrix} x' \\ y' \\ z' \end{bmatrix} = r \begin{bmatrix} cos(\theta)\, cos\,(\phi) \\ cos(\theta)\, sin\,(\phi) \\ sin\,(\theta) \end{bmatrix}$$

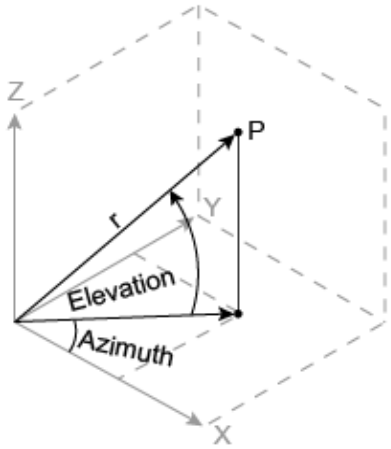

Figure 3 - Spherical to Cartesian Conversion

To properly determine the coordinates of the target within the room's coordinate plane, it was imperative to align the coordinate system of the sensor (body frame coordinate system) to that of the room (Local Coordinate System). Achieving this alignment involves a series of calculations that account for the sensor's yaw, pitch, and roll. These adjustments were critical in ensuring that the sensor's data correspond accurately to the room's coordinate plane, allowing for reliable 3D positioning. Assuming that the anchor is first rotated by an angle ψ around the *z*-axis (yaw), then by an angle θ around *y*-axis (pitch) and finally by an angle ϕ around the *x*-axis (roll) the 3*x*3 rotation matrix is given by:

$$R = R_z + R_y + R_x$$

where,

$$R_x = \begin{bmatrix} 1 & 0 & 0 \\ 0 & cos(\varphi) & -sin(\varphi) \\ 0 & sin(\varphi) & cos(\varphi) \end{bmatrix}$$

$$R_y = \begin{bmatrix} cos(\varphi) & 0 & sin(\varphi) \\ 0 & 1 & 0 \\ -sin(\varphi) & 0 & cos(\varphi) \end{bmatrix}$$

$$R_z = \begin{bmatrix} cos(\varphi) & -sin(\varphi) & 0 \\ sin(\varphi) & cos(\varphi) & 0 \\ 0 & 0 & 1 \end{bmatrix}$$

With reference to Figure 4 and considering that body-frame measurement from a sensor positioned at $A = [x_a y_a z_a]$ is $P' = [x'y'z']$ then the local coordinates $P = [xyz]$ of the target can be calculated using:

$$P = [R \cdot P'^T]^T + A$$

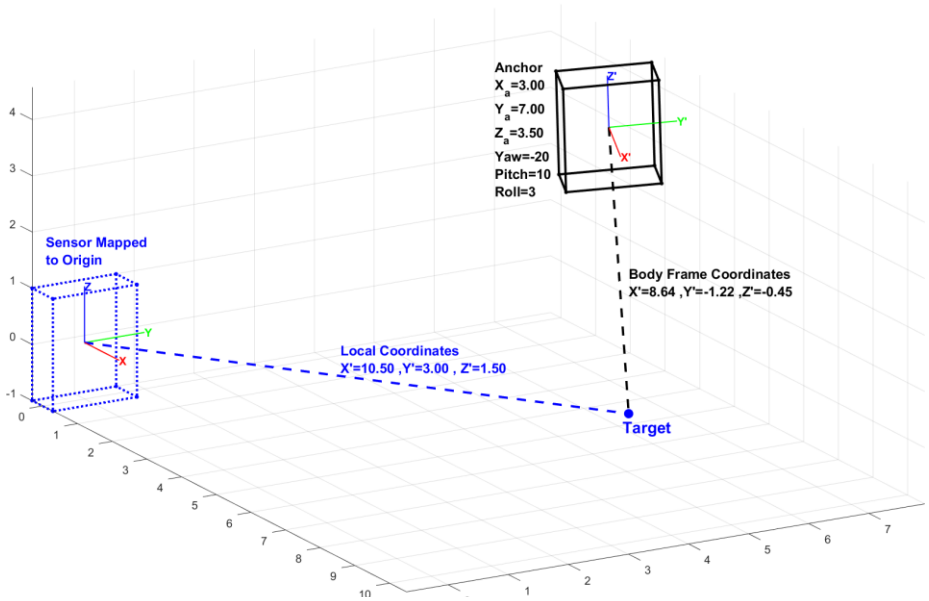

Figure 4 - Body Frame to Local Coordinates Conversion

The IWR1843BOOST was used to conduct a single sensor 3D positioning experiment, evaluating its performance over a distance of 6.5 meters. The evaluation revealed a varying level of accuracy contingent on azimuth and elevation angles. With reference to the results presented in Figure 5, when the sensor was aligned at 0 degrees azimuth, it demonstrated exceptional 3D accuracy which was slowly increasing as the distance and elevation from the target were increased. As it was expected, at large elevation angles (e.g. 45 degrees) and at long distances the sensor was failing to provide a measurement. This is indicated by the gaps in the surface plots in Figure 5. The contour plots at the bottom of each surface plot indicate the range of Distance/Elevation values that the error is below an intuitively-selected accepted 3D positioning error ($0.4m$). As it was expected the positioning accuracy appears to deteriorate faster as the azimuth angle starts increasing limiting the usability and reliability of the sensors at very low elevation and azimuth maximums. In a scenario were multiple sensors are used, one could use the range, azimuth and elevation measurements as a measure

of the reliability of the single-anchor position estimation and either use or discard the particular anchor from the entire positioning algorithm.

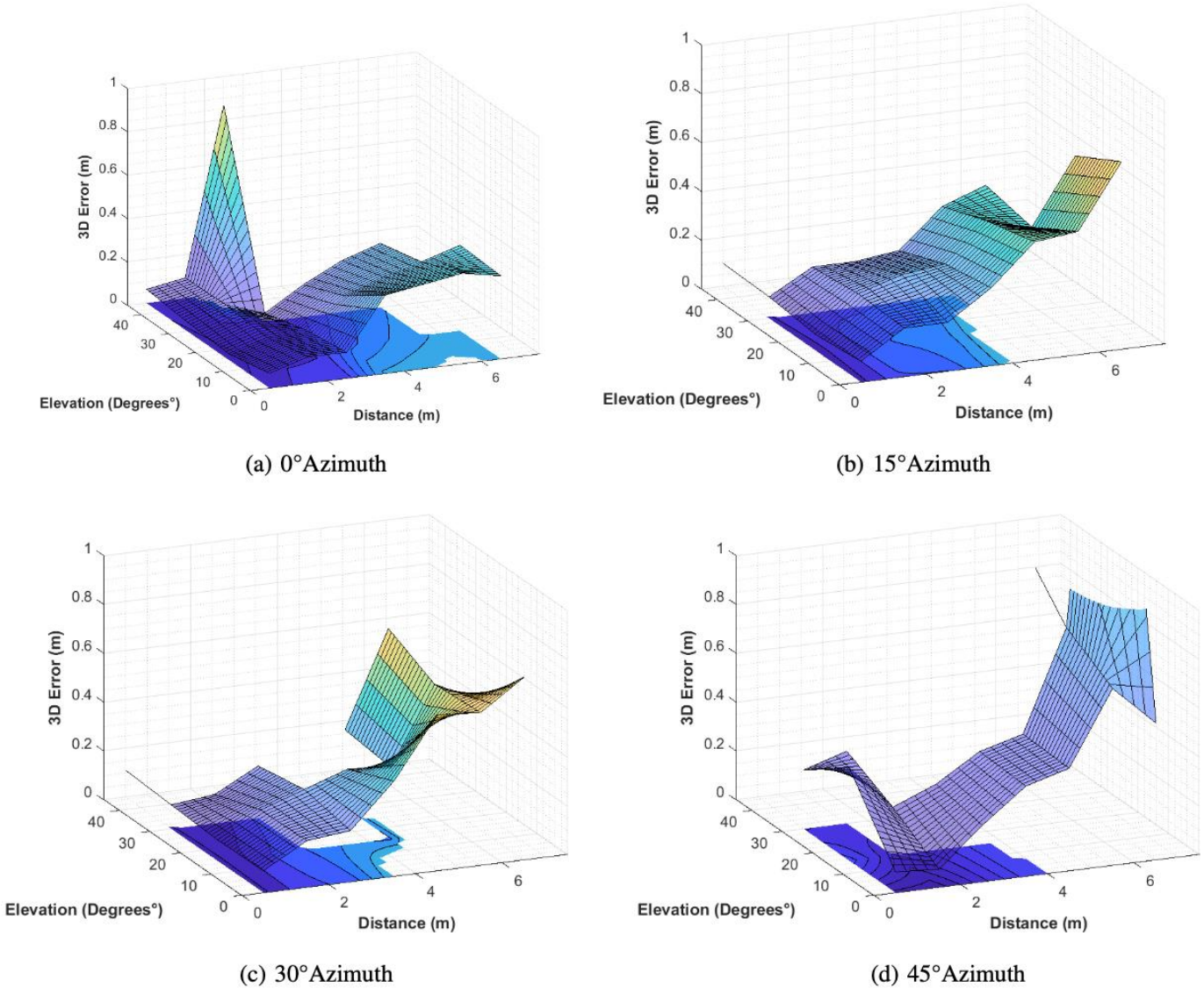

Figure 5 - IWR1843BOOST Single Sensor Positioning Accuracy

This adaptability in adjusting the sensor's coordinate system, regardless of its orientation, proved to be a pivotal advantage. It enabled us to place and orient the sensor in positions that were previously challenging due to issues related to sensor clustering. This flexibility allowed us to direct the sensor towards unconventional angles, such as placing it on the ceiling facing downward or on the floor facing upward.

2.2.2 3-DOF Multi Anchor 3D Positioning

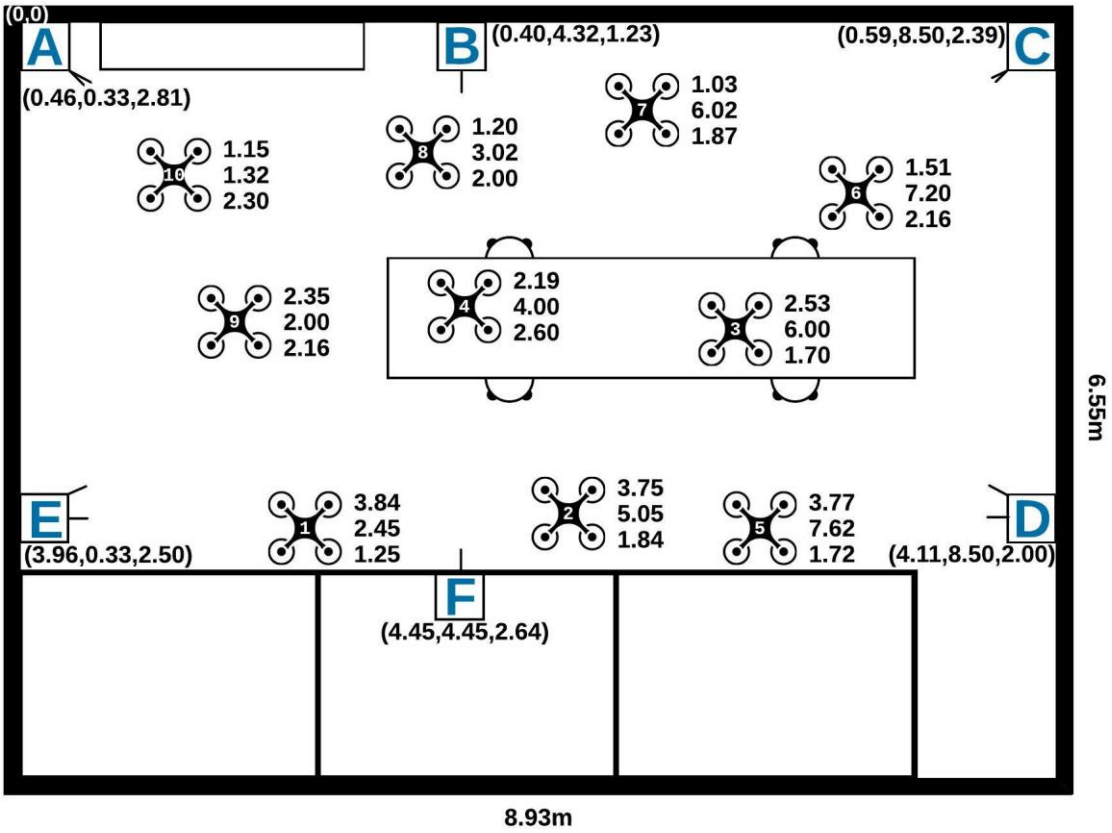

Figure 6 - mmWave 3D Positioning Experimental Setup using 3-DOF mmWave Sensors

In this experiment, a 3-DOF multi-anchor 3D positioning system was implemented using IWR1832BOOST mmWave sensors. The study involved the use of five sensors, in the environment shown in Figure 6, where two distinct setups were tested, each with slight variations. In Setup A, one sensor was placed lower than the others and faced upward, while in Setup B, a sensor was positioned higher than the rest and faced downward. Both configurations were rigorously examined using 3 different approaches: an Averaged Multi-Anchor Positioning Approach, a classical Multilateration Approach and a multiangulation approach using Angle of Departure (AoD). The obtained results can be seen in Table 5 and Table 6. The experiment consisted of a drone hovering over multiple randomly selected points at various heights. Each of the sensors would capture and position the drone, outputting the 3D coordinates *(xyz)* using the single-anchor positioning approach presented in Section 2.2.1 as well as the azimuth and elevation angling and ranging data for the Triangulation and Multilateration approaches respectively. As shown in the section, it is possible to achieve the 3D position using only one 3-DOF mmWave sensor, however this setup consisted of five, the position estimates of which were averaged to estimate the final drone position.

Averaged Multi-Anchor Approach: Capitalizing on the capability of the IWR1843BOOST sensor to perform single-angle positioning the averaged approach consists of utilizing more than one (5 in this experiment) while having their estimates averaged to estimate the target position. Our algorithm involved discarding estimates which appeared as outliers or

they have been estimated using measurements at long distances, high azimuth and elevation angles which we observed in the precision analysis are likely to cause large positioning errors. The outcomes demonstrated a remarkable precision, with an error of approximately 17*cm* observed using Setup A and 16*cm* using Setup B. The minimal disparity between the results of the two setups indicates the robustness of the system. However, it can be observed from Table 5 that the configuration where one sensor was positioned on top facing downward exhibited superior results in the *Z*-axis compared to the alternative setup. Qualitatively, we can also report that we observed that Setup B resulted in less sensor failures, resulting in more estimates being considered in the averaging process and the final calculation of the target position. Figure 7 is a visual demonstration of the positioning accuracy achieved using Setup B when the drone was flown along the trajectory indicated with a blue dotted line. Ground truth locations where available at the points indicated with a blue circle while red diamonds are the actual position estimates. Comparing these findings to a 2-DOF 3D triangulation approach presented in Section 2.1.2, it is noteworthy that the results were very similar, with a 3D error of approximately 17*cm* also. Overall, this experiment showcases the potential and reliability of the implemented system in real-world applications requiring precise 3D object localization.

Multilateration Approach: Using the ranging information from at least 4 sensors, we were able to establish the 3D position of the target using multilateration similarly to the approach described in Section 2.1.1. The results demonstrated a 3D error of 0.21*m* using Setup A and 0.86*m* using Setup B. It can be seen that the higher errors compared to the averaged approach are mostly due to high errors in the *Z*-axis, especially using Setup B. These errors are due to the fact that the sensors are positioned at relatively similar heights compared to Setup A where one sensor is positioned much lower and aimed looking up. This leads to a worsened distribution of the sensors vertically and therefore higher VDOP which as discussed in Section 3.5, leads to poor multilateration performance.

Multiangulation Approach: To implement the AoD approach, angling information (azimuth and elevation) from at least 3 sensors to the target is required to establish the 3D position of the targeted object. The formulation of this approach can be found in [23]. As it can be seen in Table 5 and Table 6, the average 3D error using the AoD approach was calculated to be around 0.22*m* using Setup A and around 0.25*m* using Setup B.

Table 5: 3-DOF Multi-Anchor 3D Positioning Results - Setup A (Y: Yaw, P: Pitch, R: Roll)

Setup A													
Point	Averaged Approach				Multilateration Approach				Multiangulation Approach				Sensor Setup
	Error XYZ *(m)*			3D Error *(m)*	Error XYZ *(m)*			3D Error *(m)*	Error XYZ *(m)*			3D Error *(m)*	
	x	*y*	*z*		*x*	*y*	*z*		*x*	*y*	*z*		
1	0.11	0.02	0.22	0.25	0.10	0.04	0.25	0.27	0.01	0.21	0.25	0.33	A Y:45°,P:15°,R:0° B Y:0°,P:-30°,R:0° C Y:-45°,P:15°,R:0° D Y:-90°,P:15°,R:0° E Y:90°,P:15°,R:0°
2	0.09	0.20	0.01	0.22	0.30	0.16	0.46	0.57	0.32	0.04	0.06	0.33	
3	0.01	0.02	0.10	0.10	0.15	0.04	0.05	0.16	0.04	0.05	0.16	0.18	
4	0.06	0.09	0.07	0.13	0.32	0.02	0.62	0.70	0.17	0.07	0.15	0.23	
5	0.09	0.14	0.01	0.17	0.09	0.10	0.31	0.34	0.10	0.00	0.06	0.11	
6	0.00	0.12	0.14	0.18	0.16	0.09	0.08	0.20	0.18	0.02	0.21	0.27	
7	0.08	0.06	0.01	0.10	0.05	0.06	0.09	0.12	0.07	0.08	0.06	0.12	
8	0.04	0.09	0.12	0.16	0.10	0.09	0.01	0.13	0.24	0.07	0.21	0.33	
9	0.07	0.11	0.02	0.13	0.03	0.09	0.08	0.13	0.02	0.05	0.09	0.11	
Avg.	***0.07***	***0.10***	***0.09***	***0.17***	***0.14***	***0.08***	***0.21***	***0.21***	***0.13***	***0.07***	***0.14***	***0.22***	
SD	***0.04***	***0.05***	***0.08***	***0.05***	***0.10***	***0.04***	***0.21***	***0.21***	***0.11***	***0.06***	***0.07***	***0.10***	

Table 6: 3-DOF Multi-Anchor 3D Positioning Results - Setup B (Y: Yaw, P: Pitch, R: Roll)

Setup B													
Point	Averaged Approach				Multilateration Approach				Multiangulation Approach				Sensor Setup
	Error XYZ *(m)*			3D Error *(m)*	Error XYZ *(m)*			3D Error *(m)*	Error XYZ *(m)*			3D Error *(m)*	
	x	*y*	*z*		*x*	*y*	*z*		*x*	*y*	*z*		
1	0.02	0.11	0.02	0.11	0.24	0.04	0.56	0.61	0.14	0.02	0.03	0.14	A Y:31°,P:15°,R:0° B Y:-58°,P:15°,R:0° C Y:-121°,P:15°,R:0° D Y:117°,P:15°,R:0° E Y:-180°,P:30°,R:0°
2	0.03	0.09	0.09	0.13	0.26	0.00	0.15	0.30	0.23	0.13	0.17	0.31	
3	0.02	0.00	0.13	0.13	0.16	0.04	0.73	0.75	0.04	0.19	0.21	0.29	
4	0.08	0.02	0.08	0.11	0.42	0.15	0.66	0.79	0.20	0.20	0.17	0.33	
5	0.13	0.02	0.02	0.13	0.09	0.11	0.30	0.34	0.06	0.11	0.06	0.14	
6	0.24	0.02	0.01	0.24	0.43	0.05	0.56	0.71	0.37	0.00	0.08	0.38	
7	0.28	0.14	0.05	0.32	0.19	0.14	1.28	1.30	0.13	0.14	0.13	0.23	
8	0.01	0.18	0.02	0.18	0.11	0.19	1.17	1.19	0.04	0.19	0.05	0.20	
9	0.06	0.02	0.08	0.10	0.11	0.01	1.75	1.75	0.24	0.12	0.01	0.27	
Avg.	***0.10***	***0.06***	***0.05***	***0.16***	***0.22***	***0.08***	***0.79***	***0.86***	***0.16***	***0.12***	***0.10***	***0.25***	
SD	***0.10***	***0.06***	***0.04***	***0.07***	***0.13***	***0.06***	***0.51***	***0.47***	***0.11***	***0.07***	***0.07***	***0.08***	

The experiment consisted of a drone hovering over multiple randomly selected points at various heights. Each of the sensors would capture and position the drone outputting the 3D coordinates (*xyz*) using the single-anchor positioning approach presented in the previous paragraph 2.2.1. Depending on how many anchors detect the drone there were that many estimates of the target. Our algorithm involved discarding estimates which appeared as outliers or they have been estimated using measurements at long distances, high azimuth and elevation angles which we observed in the precision analysis are likely to cause large positioning errors. The outcomes demonstrated a remarkable precision, with an error of approximately 17*cm* observed using Setup A and 16*cm* using Setup B. The minimal disparity between the results of the two setups indicates the robustness of the system. However, it can be observed from Error! R

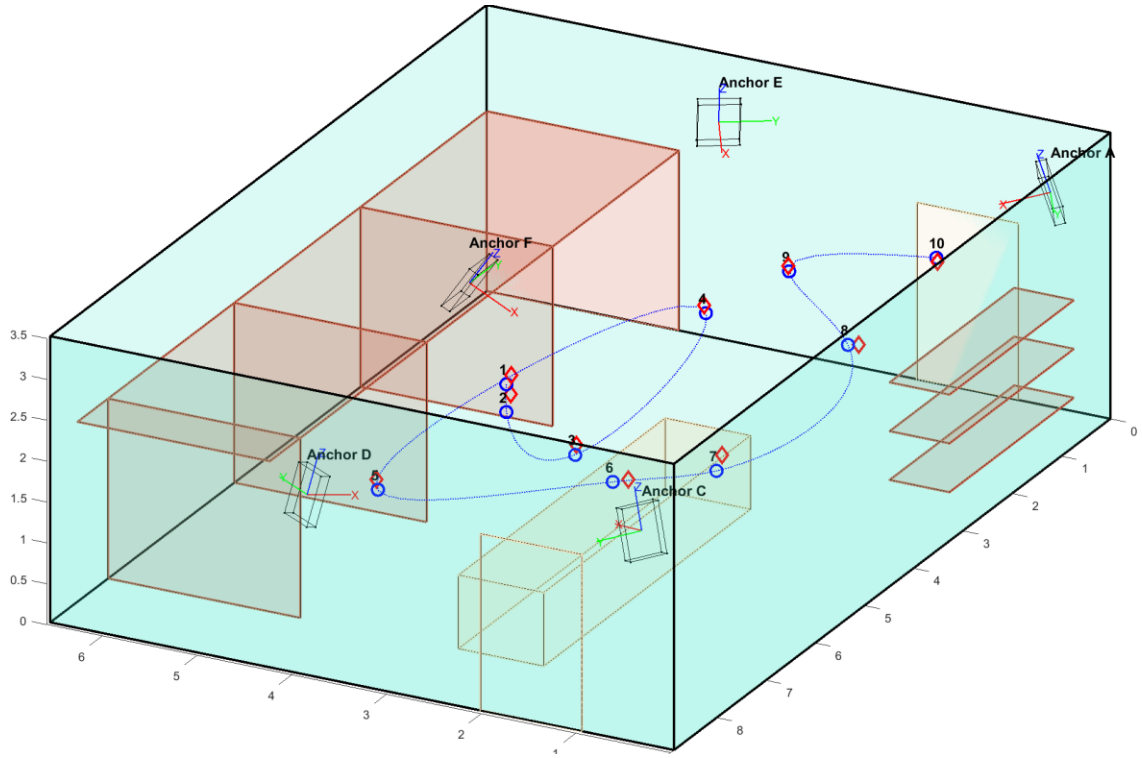

Figure 7 - 3D Positioning using Multiple 3-DOF mmWave Anchors. Blue circles indicate ground truths and red diamonds estimated positions

eference source not found. that the configuration where one sensor was positioned on top and faced downward exhibited superior results in the *z*-axis compared to the alternative setup. Qualitatively, we can also report that we observed that Setup B resulted in less sensor failures, resulting in more estimates being considered in the averaging process and the final calculation of the target position. Figure 7 is a visual demonstration of the positioning accuracy achieved using Setup B when the drone was flown along the trajectory indicated with a blue dotted line. Ground truth locations where available at the points indicated with a blue circle while red diamonds are the actual position estimates.

Comparing these findings to a 2-DOF 3D triangulation approach, it is noteworthy that the results were very similar, with a 3D error of approximately 17*cm* also. Overall, this experiment showcases the potential and reliability of the implemented system in real-world applications requiring precise 3D object localization.

2.3 Simulation Analysis

Using the single target 3DOF positioning simulator developed in this project (see chapter 3 in deliverable D4.1) a more comprehensive analysis was conducted in the same simulated environment utilizing more points. The anchors were defined to be at the locations defined in Setup A and Setup B in section 2.2.2. 3 cases were considered. The case were outliers are not considered in the simulation, the case were outliers are assumed to exist in the measuremrenets collected from each sensor and one in which the outliers are filtered out. In all cases a drone is instructed to fly over a predefined route that consists of 200 locations and each sensor returns an errorneous measurement based on the precision analysis error model we estimated through the Precision Analysis of the 3DOF sensor.

2.3.1 No Outliers

In this case outliers are excluded from the simulation.

2.3.1.1 Setup A

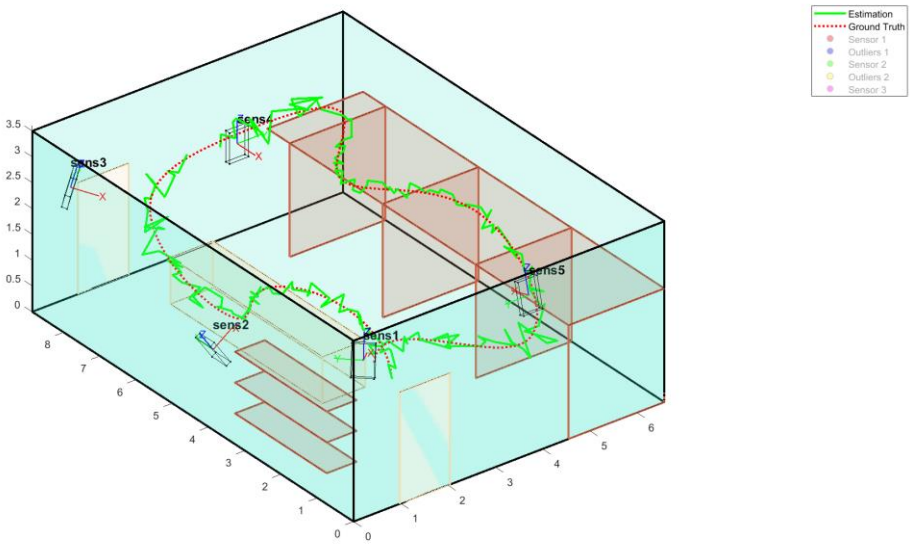

Figure 8: Simulation of Setup A with out Outliers

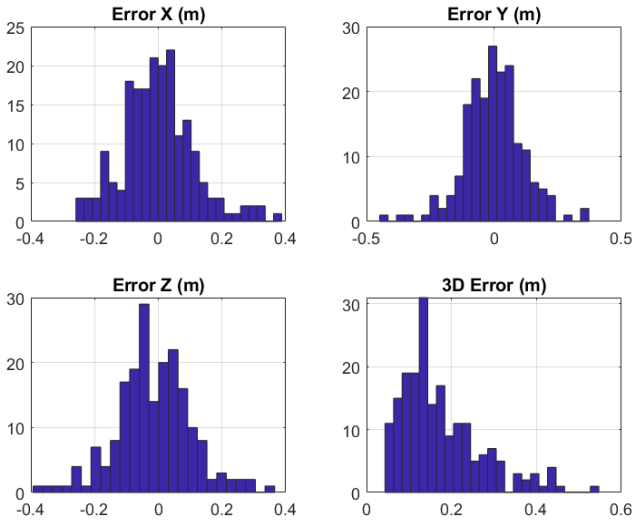

Figure 9: Positioning Error Profile of Simulation without Outliers in Setup A

As seen from Figure 8 and Figure 9 when outliers are not considered in the simulation then the error performance is quite good with a 3D error averaging at **17.65cm** (where Error X=8.5cm Error Y=8.7cm Error Z=9.3cm. A notable observation is the fact that between Anchor 3 and 4 the system fails to return a position estimation due to the absence of reliable measurements from all the 5 anchors (either due to high elevation or azimuth angle or long distances to the target).

2.3.1.2 Setup B

Setup B as adjusted to optimize the positioning accuracy in the centre of the room by adjusting the orientations of the sensors while moving sensor 2 in a new location

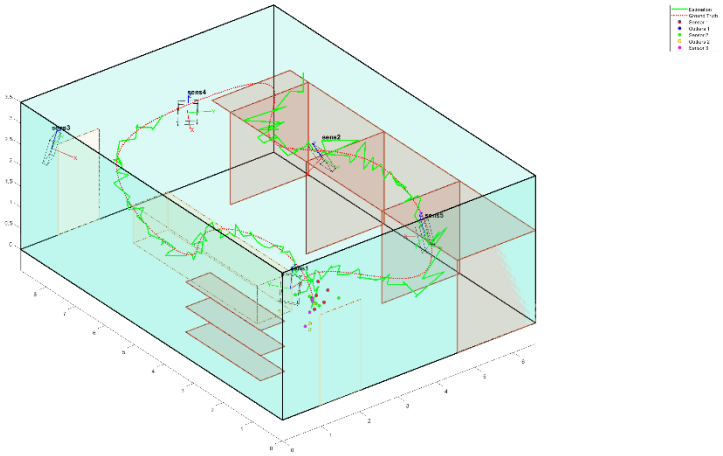

Figure 10: Simulation of Setup B with out Outliers

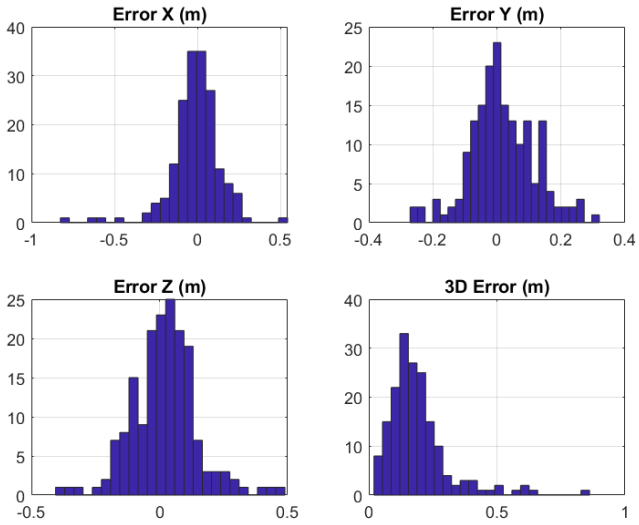

Figure 11: Positioning Error Profile of Simulation without Outliers in Setup B

As seen from Figure 10 this constellation of sensors fixes the problem with the lack of position estimation between sensor 3 and 4 but instead it generates a new issue between sensor 2 and 3. This verifies that careful placement and orientation of anchors is required in order to achieve good results everywhere within the room. Figure 11 indicates again a very good positioning accuracy with the 3D error averaging at **19.02cm** (where Error X=10.32cm Error Y=7.8cm Error Z=9.7cm). The minor increase compared to the Setup A can be attributed to the high errors around the vicinity of sensor 2 where the drone was instructed to fly at the back of the sensor resulting higher than usual errors.

2.3.2 Outliers considered

The simulations presented in the previous section are rather unrealistic as each sensor does not just return a single measurement but instead it returns a cluster of measurements around the flying object as well as some random outliers around the room. These outliers have significant effect on on the positioning accuracy if not filtered out. This section presents the results for the two setups when a number of outliers are assumed to be generated from each sensor. These outliers are generated statistically in the following way: (1) outliers around each sensor which could be due to the cross-sectional area of the sensor. The number of these outliers is a normal distribution with mean 6 and standard deviation 3. The distance from the measurement for each outlier is assumed to be also a normally distributed with mean of 30cm and standard deviation of 20cm. (2) outliers randomly appearing within the boundaries of the entire room. The total number of these outliers per anchor is a normal distribution with mean 3 and standard deviation 2.

2.3.2.1 Setup A

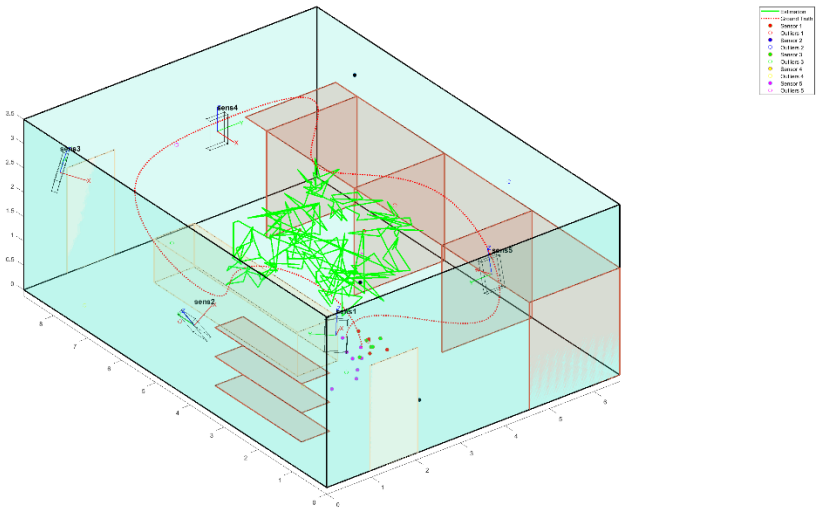

Figure 12: Simulation of Setup A with out Outliers

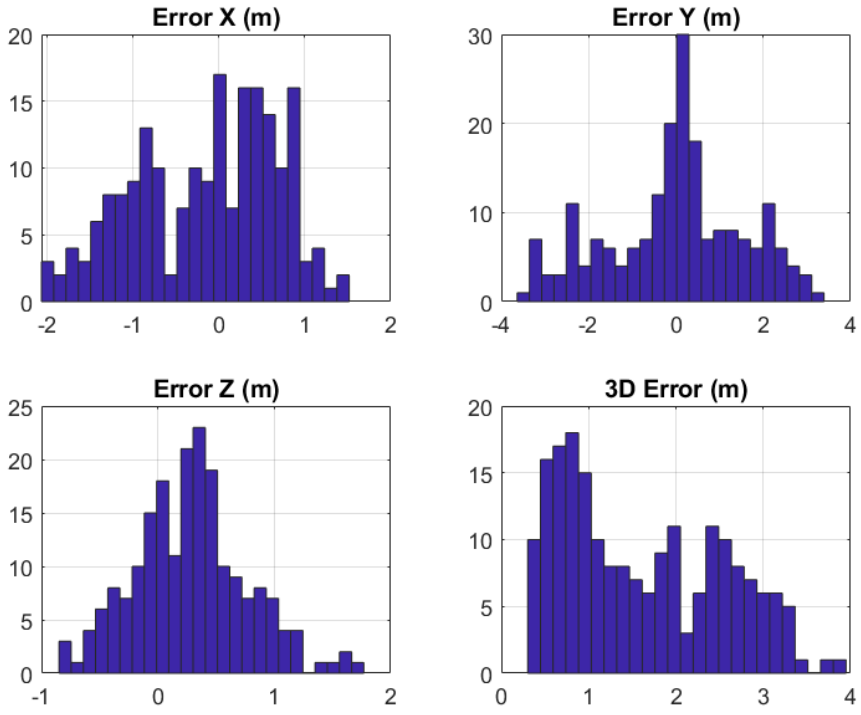

Figure 13: Positioning Error Profile of Simulation without Outliers in Setup A

The results indicate a noticeable degradation of the positioning performance with the 3D positioning error averaging at 1.61m (where Error X=0.69m Error Y=1.19m Error Z=0.44m)

2.3.2.2 Setup B

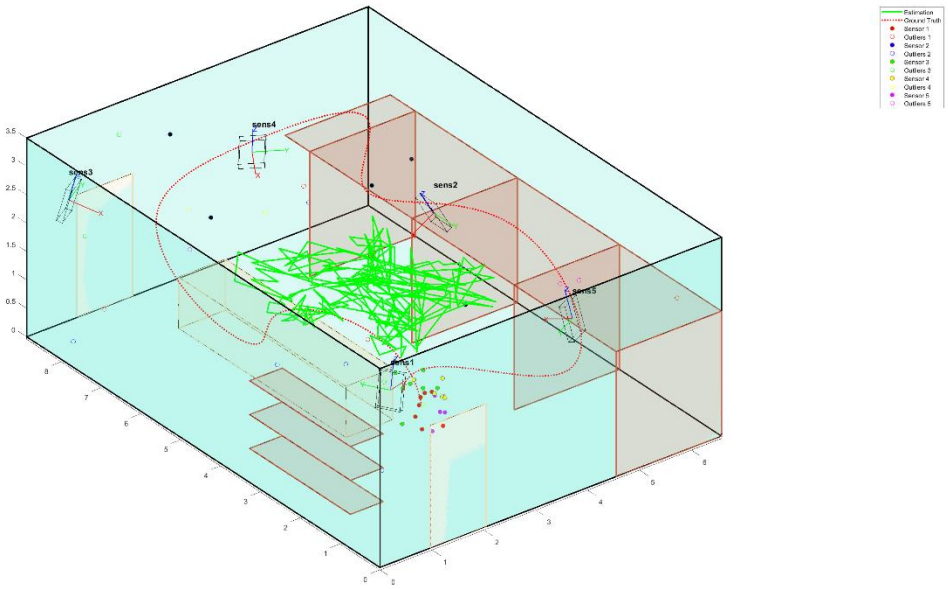

Figure 14: Simulation of Setup A with out Outliers

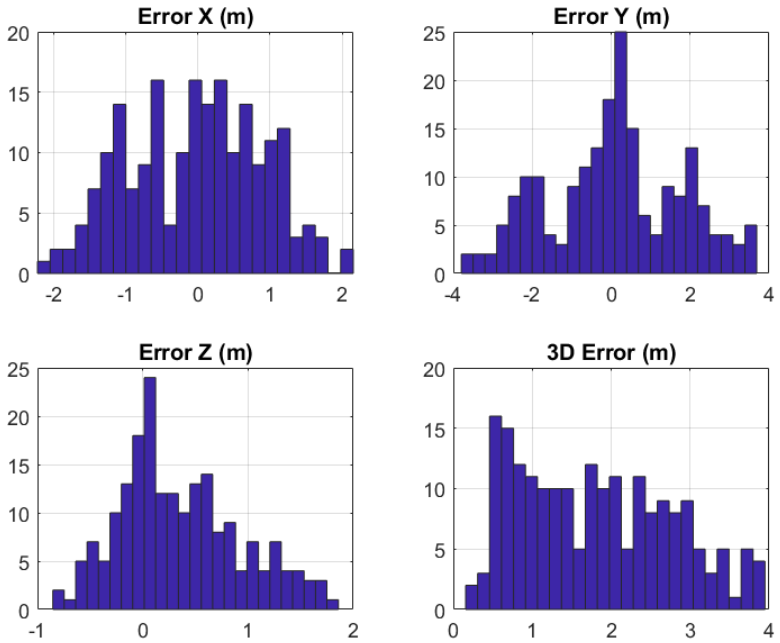

Figure 15: Positioning Error Profile of Simulation without Outliers in Setup A

Similar performance in Setup B is observed with the 3D positioning error averaging at 1.8m (where Error X=0.8m Error Y=1.32m Error Z=0.53m)

2.3.3 Outliers considered and Filtered

As seen in section 2.3.2 the presence of outliers around the target as well as the random outliers around the room considerable degrade the positioning performance. To improve the situation some form of filtering of these outliers is required. In this work, this filtering is done in two steps: (1) any measurement that appears to be at an azimuth angle bigger than 35 degrees or an elevation bigger than 20 degrees at a distance bigger tan 4 meters (based on the precision analysis) is discarded (2) a dbscan clustering algorithm is used on the consolidated set of measurement points from all the sensors to remove the outliers. dBscan performs clustering by identifying candidates that are within a certain radius from each other. It takes as input the minimum number of candidates required to form a cluster and the maximum distance between them. In our simulations the minimum number of candidates is set to 5 and the minimum distance between the is set to 0.5m. The results below indicate a significant improvement compared to the ones in the previous section.

2.3.3.1 Setup A

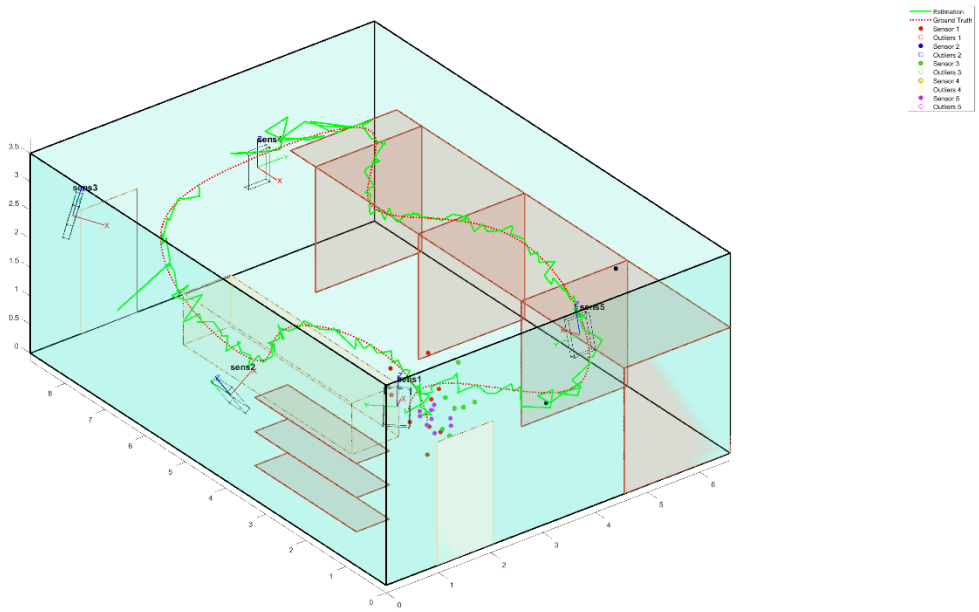

Figure 16: Simulation of Setup A with out Outliers

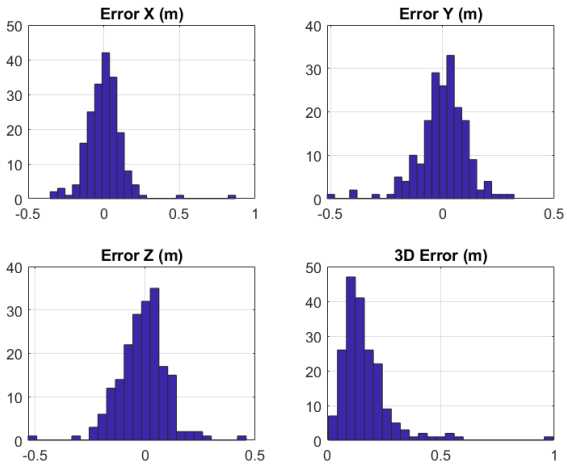

Figure 17: Positioning Error Profile of Simulation without Outliers in Setup A

A significant improvement is noted in Setup A with 3D positioning error averaging at 16.34cm (where Error X=8.3cm Error Y=8cm Error Z=8cm)

2.3.3.2 Setup B

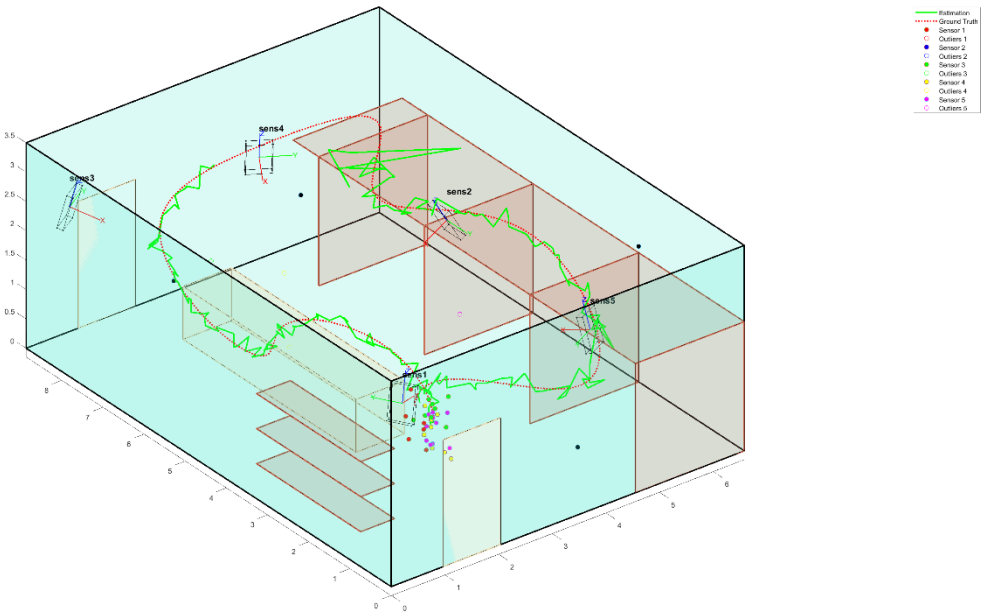

Figure 18: Simulation of Setup A with out Outliers

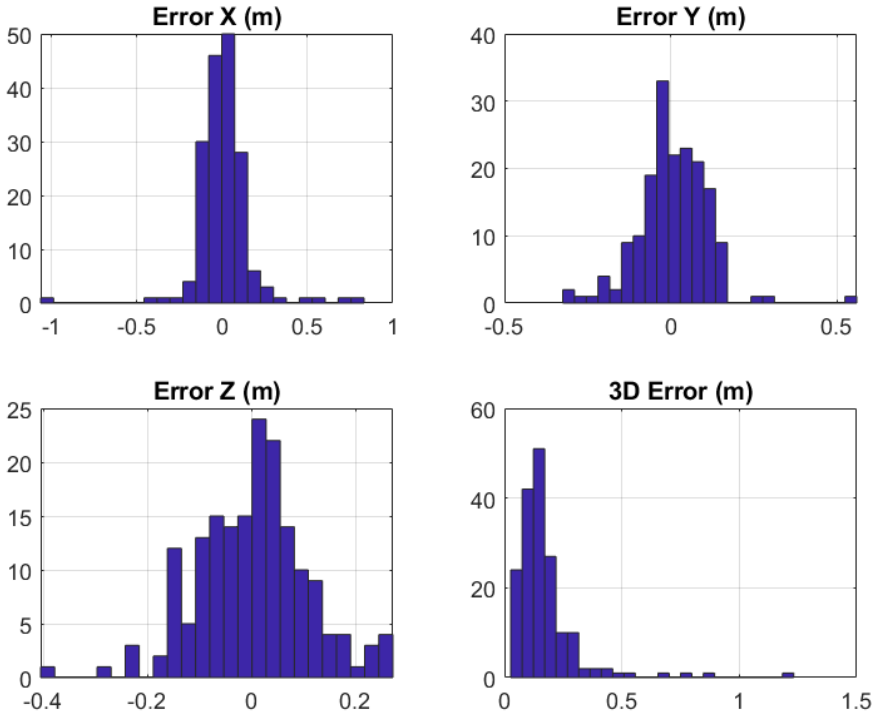

Figure 19: Positioning Error Profile of Simulation without Outliers in Setup A

Similar performance in Setup B is observed with the 3D positioning error averaging at 17.32cm (where Error X=10cm Error Y=8cm Error Z=8.3cm)

2.4 Critical Discussion

The results of the 2-DOF precision analysis and positioning estimations highlight the potential of mmWave technology for achieving range and angle measurement precision and thereafter high 3D positioning accuracy. The precision analysis revealed that out of the two sensor types that were used the Texas Instruments sensor outperformed the Infineon one in terms of range and angle measurement precision at a wider field of view. Due to the fact that the Infineon sensor is only able to identify objects up to a 20-degree angle, it becomes evident that this sensor is not appropriate for a positioning system where at least 4 sensors are required to cover the visibility of an entire room. On the other hand, TI sensor has shown very promising results, showcasing ranging precision of 0.17m at 0 degrees and a capability of identifying an object at 60 degrees with an accuracy of 0.3m up to 6m. This makes the IWR1642BOOST sensor a good choice for a 3D positioning system.

The 3D positioning estimation using the 2-DOF sensor was done using both a 3D multilateration and a triangulation approach. The multilateration approach demonstrated a relatively high 3D positioning error of 0.8m in the z-axis estimation. This indicated the challenges associated with accurately estimating the z-axis using multilateration alone. To address these limitations in z-axis estimation, a 2D triangulation approach utilizing azimuth angles from 3 sensors

was used combined with a lateration approach to estimate the height utilizing sensors placed on top of each other. Although only one additional sensor is required to be placed at a higher altitude above one of the existing sensors to be able to estimate the height, we have deployed 2 sets at the two corners of the room to ensure sufficient measurements in case one of these fails to return measurements due to either blockages or long distances. This modification in the sensor setup resulted in a reduction of the z-axis error down to $0.11m$, leading to an overall decrease in the 3D positioning error down to $0.17m$. The errors in the x and y axes also improved, indicating the effectiveness of the triangulation approach in precise 3D positioning estimation.

Transitioning to the 3-DOF sensor, the limitations encountered with the 2-DOF sensor, including the implementation requirements of various multilateration and triangulation techniques, were overcome by leveraging the enhanced capabilities of the 3-DOF sensor to measure the elevation of the target in addition to the distance and azimuth angle. This sensor streamlined the 3D positioning process by directly outputting the 3D coordinates of the detected object, eliminating the need for intricate multi-step methodologies. While the precision analysis demonstrated comparable results to the 2-DOF sensor, a significant advancement was noted in the expanded field of view. The 3-DOF sensor introduced an elevation angle measurement capability, enabling single-anchor 3D positioning, offering more comprehensive spatial coverage when multiple sensors are placed around the room. The utilization of multiple 3-DOF anchors demonstrated a 3D positioning accuracy of $16cm$ as well as notably improved the system's efficiency, leading to quicker response times and smoother overall functionality.

Comparing the results mentioned in Section 1 with the findings in (Ojas Kanhere, 2018) and (Hao, et al., 2022), it is evident that both our approaches yielded a similar level of accuracy. In (Ojas Kanhere, 2018), the authors achieved positioning accuracy ranging from $16cm$ to $3.25m$ using the AoA technique in an open space while the authors of (Hao, et al., 2022) demonstrated an accuracy of $15cm$. Despite the fact that we were operating in a more cluttered environment, we achieved an accuracy of $16cm$, which is comparable to the aforementioned works.

3 Challenges

During the development and setup of the positioning system described above, several challenges have emerged regarding the usage of mmWave sensors which could potentially cause significant difficulties when these are used for positioning. This section describes all these challenges and subsequently explains the solutions we implemented to overcome them.

3.1 Accuracy and Sensing

Although mmWave sensors have been introduced to be used mainly for ranging measurements for the automotive industry, they have emerged as a promising radar-like technology for indoor positioning applications due to their high accuracy in estimating distance (and angles) to objects mainly because of the availability of a very wide bandwidth on

mmWave frequencies and the availability of phase antenna arrays on the sensor board. However, the accuracy of mmWave sensors is highly dependent on the sensing conditions, such as the scattering caused due to reflective surfaces, the angle of incidence, and the distance between the sensor and the target object. In addition, the complexity of the indoor environment including multipath effects, can affect the accuracy of mmWave sensing. Therefore, careful consideration of the sensing conditions and the deployment of mmWave sensors is essential to achieve high accuracy in indoor positioning applications. Our experimentation has indicated that the presence of metallic objects in the close vicinity of the target or within the field of view of the sensor causes problems.

3.2 Stationary Positioning

In addition to the sensing constraints, the fact that these sensors rely strongly on the Doppler-effect principle, challenges emerge when stationary targets need to be detected. To be sensed by a mmWave radar sensor, an object must be constantly in motion for the sensor to be able to detect the Doppler shift and distinguish it from stationary objects and background noise. To overcome this challenge, researchers are currently exploring several approaches. One promising solution could be the fusion of mmWave data with information collected from inertial sensors. For our experiments, this limitation was overcome by making the drone make small movements around the target location, collecting multiple measurements from a single location which were then averaged.

3.3 Multi-object Detection/Clustering

An inherent limitation of the off-the-shelf mmWave sensors compared to systems that use receivers on the target is the fact that they operate based on the radar principle reducing the capability of identifying correctly specific objects. The mmWave sensor emits electromagnetic waves at high frequencies that bounce off surrounding objects and return as echoes. By analyzing the time delay and amplitude of these echoes, the sensor can determine the location and characteristics of the objects in the environment relative to each sensor. These echoes, however, can become mixed together in complicated environments with multiple objects, making it difficult to differentiate and identify specific objects. This becomes especially more challenging when using multiple sensors to identify a position of a specific object in the presence of other moving or stationary objects. The solution to this multi-object identification is clustering. Literature reports various clustering approaches that can be used for this purpose (B. Antonescu, 2019) (H. He, 2021) (M. T. Moayyed, 2019).

The clustering technique used in this work to identify a specific target is known as the z-score method (Sumathi, 2012), which is widely employed for identifying and managing outliers in datasets. This method begins by calculating the mean and standard deviation of the dataset and then computes the z-score for each data point, measuring its deviation from

the mean in terms of standard deviations. By establishing a threshold, typically based on a certain number of standard deviations away from the mean, outliers can be identified and subsequently removed from the initial detected objects list to obtain a new filtered list of clustered points.

The ability of the IWR1642BOOST sensor to measure the relative range and azimuth of a detected object facilitates this clustering process as it allows the estimation of the relative (x, y) coordinate of the target. As this target is detected from multiple sensors its relative coordinates need to be converted to absolute ones by utilizing the rotation/translation equations shown below in which θ is the absolute orientation of the sensor and x_{trans}, y_{trans} are the 2D coordinates of each sensor relative to the chosen 0,0 point. Once this is done, the measurements from each sensor correspond to the same axes system, and their (x, y) coordinates can be matched to identify the range/angle measurements from the multiple sensors to the same object.

$$x_{abs} = xcos\theta + ysin\theta + x_{trans}$$
$$y_{abs} = -xsin\theta + ycos\theta + y_{trans}$$

The analogous clustering process for IWR1843BOOST sensors closely mirrors the aforementioned methodology. Utilising the inherent ability to measure the relative range and azimuth, these sensors facilitate the estimation of relative (*x, y, z*) coordinates for detected objects. Similar to the IWR1642BOOST, these relative coordinates are then translated to a common axis system by utilising the equations mentioned in Section 2.2.1, ensuring uniformity across sensor data. Subsequently, the z-score method is employed once again to eliminate outliers and identify the object of interest.

The Z-score clustering method, while effective in isolating a singular object amidst data from multiple mmWave sensors, faces limitations when it comes to identifying multiple objects within a given space. Recognizing this shortfall, further exploration of clustering approaches was undertaken to enhance the method's capability in discerning multiple objects.

In pursuit of this goal, the implementation of multi-object clustering solutions has proven to be a critical endeavor, offering enhanced accuracy and efficiency in tracking moving objects. Among the employed clustering techniques, three notable approaches were explored: K-means clustering, DBSCAN (Density-Based Spatial Clustering of Applications with Noise), and a hybrid solution that cleverly combined aspects of both. To evaluate the effectiveness of these clustering techniques, experimentation was conducted in a controlled laboratory environment. Hanging basketballs at known locations and heights provided a simulated representation of moving objects in three-dimensional space.

Point	K-means Approach				DBSCAN Approach				Hybrid Approach			
	Error XYZ (m)			3D Error (m)	Error XYZ (m)			3D Error (m)	Error XYZ			3D Error (m)
	x	*y*	*z*		*x*	*y*	*z*		*x*	*y*	*z*	
1	0.16	0.06	0.11	0.21	0.17	0.04	0.08	0.20	0.14	0.03	0.16	0.21
2	0.13	0.06	0.22	0.26	0.07	0.11	0.19	0.23	0.11	0.04	0.22	0.25
3	0.14	0.19	0.16	0.29	0.12	0.09	0.09	0.17	0.15	0.20	0.25	0.35
4	0.33	0.13	0.34	0.49	0.29	0.10	0.36	0.47	0.21	0.17	0.41	0.49
5	0.17	0.13	0.19	0.28	0.12	0.05	0.18	0.22	0.11	0.08	0.34	0.37
Avg.	***0.19***	***0.11***	***0.20***	***0.30***	***0.16***	***0.08***	***0.18***	***0.26***	***0.14***	***0.10***	***0.28***	***0.33***
SD	***0.08***	***0.06***	***0.08***	***0.11***	***0.08***	***0.03***	***0.11***	***0.12***	***0.04***	***0.08***	***0.10***	***0.11***

3.3.1 K-means Clustering Approach

The K-means clustering approach, a classic method widely applied in data science, involves partitioning a dataset into K distinct, non-overlapping subsets or clusters. In the context of mmWave sensor data, this technique was employed to group spatial coordinates of the detected objects. The algorithm iteratively assigns data points to the nearest cluster centroid based on Euclidean distance, optimizing until convergence. The resulting clusters represent distinct entities in the 3D space, aiding in precise localization of the targets. K-means requires the user to specify the number of clusters (K) in advance. Determining the optimal value for K can be challenging, and choosing an incorrect K may result in either over-segmentation or under-segmentation of the data which can lead to incorrect positioning results. The results of the K-means clustering approach can be seen below:

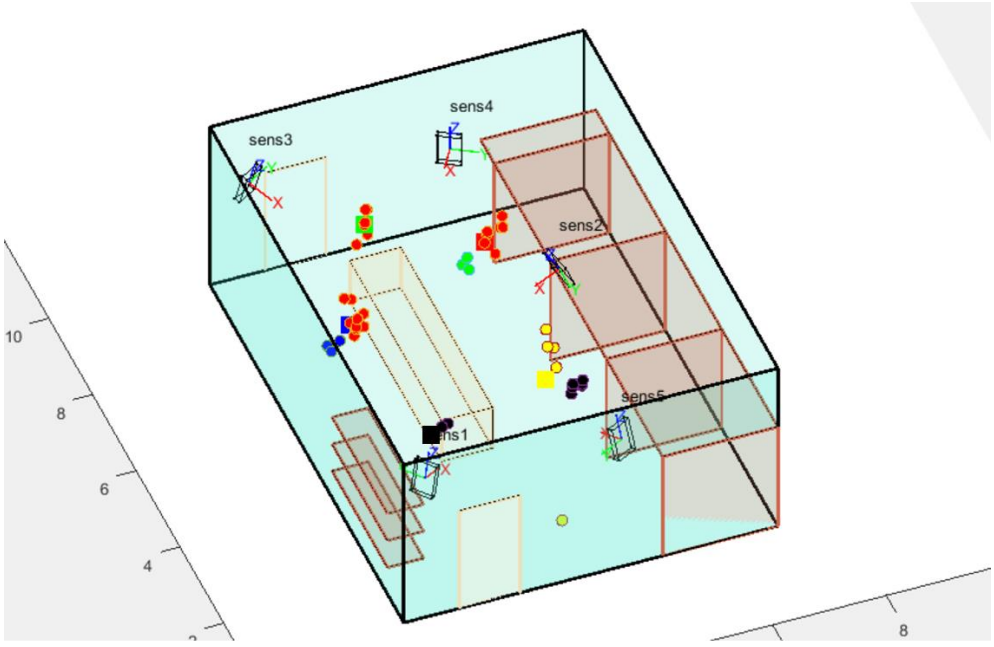

Figure 20: K-means Clustering (3D View)

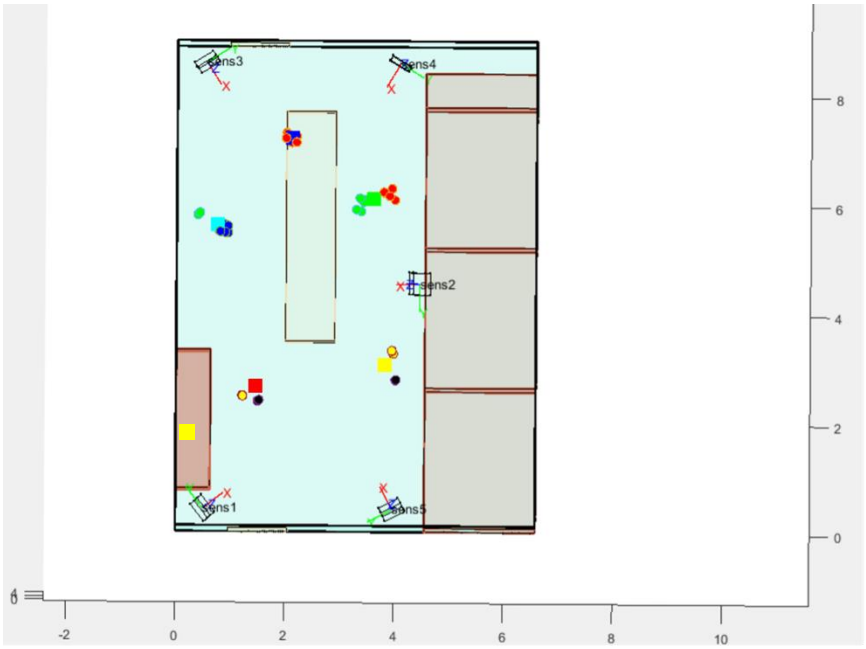

Figure 21: K-means Clustering (Top View)

3.3.2 DBSCAN Clustering Approach

DBSCAN clustering approach operates on the principle of density, identifying clusters based on regions with a higher concentration of data points. Unlike K-means, DBSCAN can discover clusters of varying shapes and sizes, making it robust in scenarios where objects may exhibit irregular movement patterns. Also, DBSCAN does not require a manual input of the amount of clusters which is a massive advantage in cases where there are unknown amount of objects to identify. The algorithm defines core points, border points, and noise points, allowing for the flexible detection of objects in a dynamic environment. The results of the DBSCAN clustering approach can be seen below:

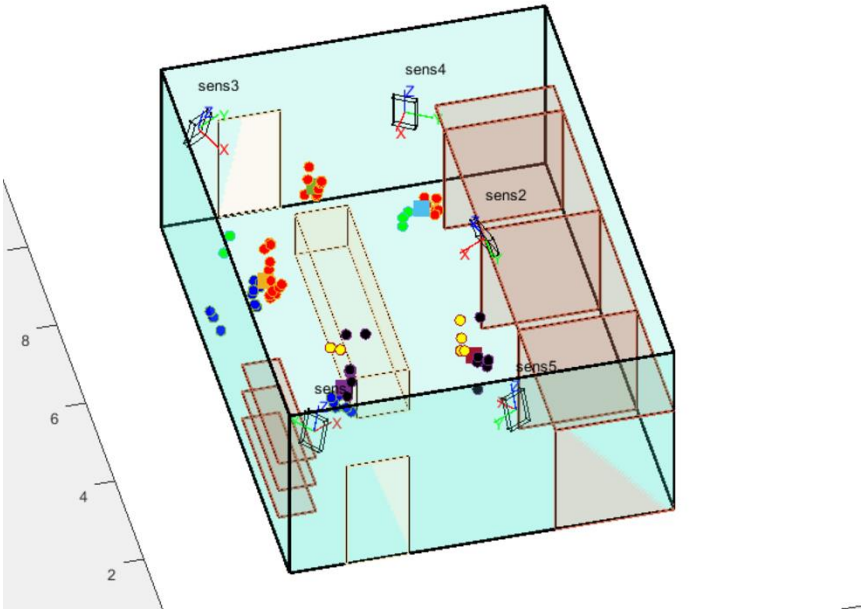

Figure 22: DBSCAN Clustering (3D View)

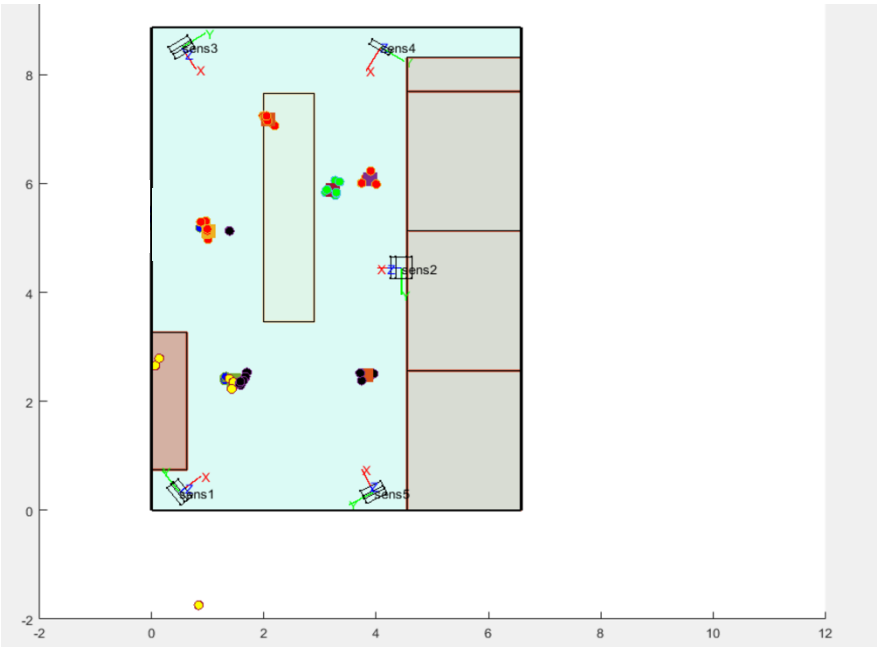

Figure 23: DBSCAN Clustering (Top View)

In the application of DBSCAN, defining meaningful parameters is pivotal for effective cluster identification. Two key parameters, namely the minimum number of points required for a region to be considered a cluster and the maximum distance (or diameter) between points within a cluster, play a crucial role.

For our specific implementation, we have set the minimum points parameter to 4. This implies that a cluster must consist of at least four data points to be recognized as a distinct group. This threshold helps filter out noise or outliers that may not contribute significantly to the density of a cluster. Additionally, we have specified a maximum distance of 0.4m as the diameter for points within a cluster. This parameter, often denoted as ε (epsilon), determines the spatial extent of a cluster. Points within this distance of each other are considered neighbors and contribute to the density of the cluster. Setting ε appropriately ensures that clusters are formed based on the local density of points, making DBSCAN robust to varying cluster shapes and sizes.

3.3.3 Hybrid Clustering Approach

The hybrid solution explores the leveraging of strengths of both K-means and DBSCAN. DBSCAN excels in identifying clusters of varying shapes and densities by defining clusters as regions with a sufficient density of data points. It does not require a predefined number of clusters and can uncover outliers as noise points. By integrating DBSCAN with K-means, the hybrid method refines the initial cluster assignments produced for the K-means, allowing for more accurate and flexible clustering.

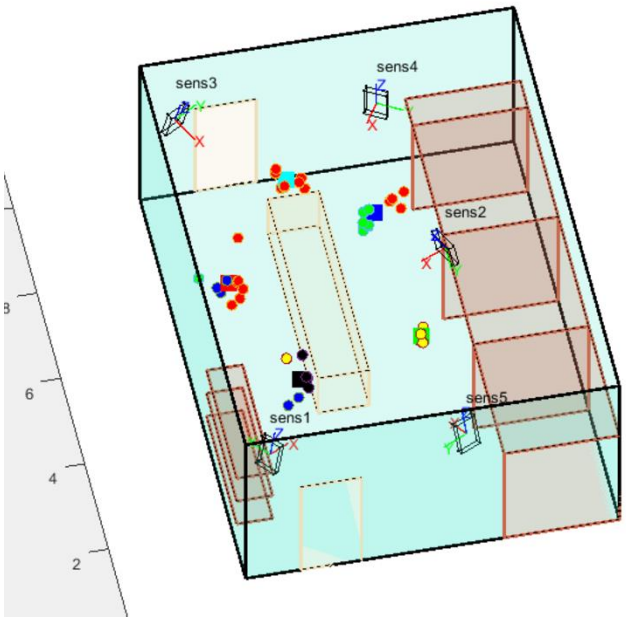

Figure 24: Hybrid Clustering (3D View)

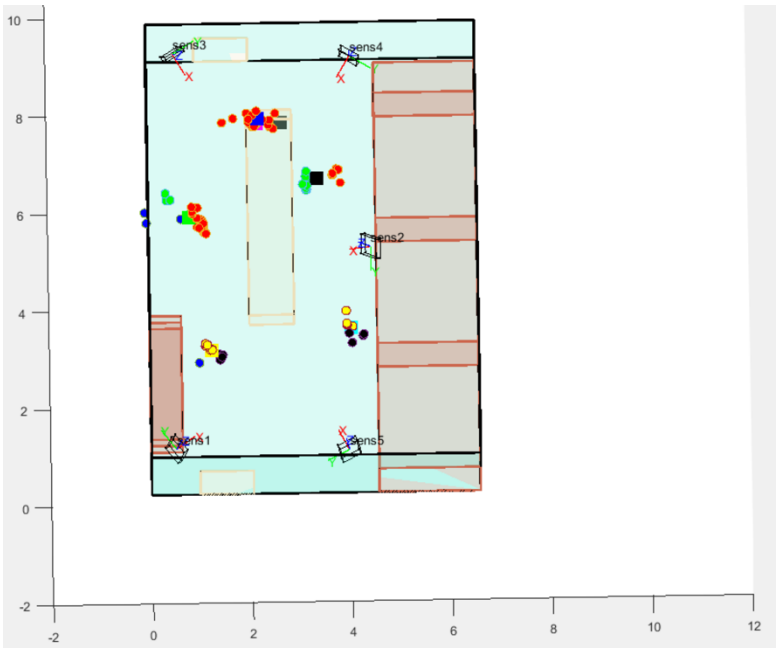

Figure 25: Hybrid Clustering (Top View)

3.3.4 Discussion

The experimental evaluation of three distinct clustering methods within the laboratory setting provided valuable insights into their performance across five simultaneously tested points, which were strategically placed at random locations throughout the lab. Among the tested methods, DBSCAN emerged as the most robust and accurate, boasting an impressive average accuracy of approximately 0.26 meters across the five points. In contrast, the K-means clustering method exhibited a slightly higher average error, hovering around 0.3 meters. Notably, the K-means approach encountered challenges when confronted with scenarios where the five points lacked clear distinguishability. In such instances, the algorithm would mistakenly identify multiple clusters within one since the preset amount of clusters is set into the algorithm. This led to the undesirable scattering of clustering points and consequent inaccuracies. Surprisingly, the hybrid clustering approach, which incorporates elements of the K-means method, proved to be the least effective among the three tested methods. It demonstrated an average accuracy of approximately 0.33 meters, indicating a higher degree of deviation compared to both DBSCAN and K-means. This diminished performance is attributed to the inherent accuracy issues stemming from the reliance on the K-means algorithm within the hybrid approach. Furthermore, the hybrid approach mirrored the challenges faced by the standalone K-means method, particularly in scenarios where the inherent characteristics of the data led to indistinct clustering boundaries. The amalgamation of clustering techniques in the hybrid model did not yield a significant improvement in accuracy, raising questions about the practical efficacy of such a combination.

3.4 Timing Synchronisation

Timing synchronization is critical in mmWave positioning systems that use multiple sensors to accurately determine the location of objects. When multiple sensors are used, they must be synchronized so that they can collectively capture and analyze the echoes returned from the environment. If the sensors are not synchronized, the echoes may arrive at different times, leading to incorrect and inconsistent measurements, which can result in inaccurate positioning data. The timing synchronization ensures that the sensors are accurately aligned in time, allowing them to capture the echoes simultaneously and consistently. Therefore, timing synchronization is critical to the performance and accuracy of mmWave positioning systems.

To achieve timing synchronization, a timestamp was placed at the beginning of each data string. The timestamp corresponds to the exact recording time, allowing for accurate alignment with the real-time clock. By matching these timestamps with the current time, the data strings within a specific timeframe were then organized into a list. Once the data string list is established, it is then filtered using the clustering technique mentioned previously and utilized to identify a specific object within the environment. At the beginning of each positioning session all the computers/Raspberries in the setup update their time using the same universal clock over the Internet.

3.5 Placement and Orientation of the Sensors

When it comes to maximizing the effectiveness of mmWave radar devices in capturing the best field of view for a given scene of interest, several key best practices come into play. These practices are particularly crucial when dealing with varying room dimensions and aiming to calculate the most optimal sensor orientation to cover the majority of a room. Firstly, it's essential to consider the room dimensions. The size and shape of the space significantly impact the placement and angle of mmWave sensors. In larger rooms, positioning sensors in multiple corners or along the walls can help achieve better coverage. In contrast, smaller rooms may require a more centralized placement to prevent blind spots. Additionally, understanding the reflective properties of the room's surfaces, such as walls, floors, and objects within the room, can aid in optimizing sensor placement. These reflective surfaces can impact the propagation of radar waves and affect the device's ability to detect objects accurately. When aiming to capture the majority of the room from a corner, to maximize coverage, angling the radar device in a way that covers a wide field of view is crucial. This can often be achieved by tilting the sensor downwards slightly from the corner and orienting it to cover both the horizontal and vertical dimensions of the room. Adjusting the sensor's vertical tilt allows it to detect objects closer to the floor and higher up, ensuring comprehensive coverage within the room.

Moreover, in scenarios where precision is paramount, employing multiple mmWave radar devices with varying angles and orientations can be beneficial. These devices can complement each other's coverage and reduce the likelihood of

missing objects or obstructions. When setting up a mmWave multilateration positioning system, it is essential to pay attention to DOP and specifically VDOP when trying to achieve 3D positioning accuracy. A key approach to optimizing DOP involves strategically selecting and configuring the positioning of the sensors in the system. By optimizing the spatial distribution of these sensors, the geometric configuration is enhanced, leading to lower DOP values. This, in turn, results in improved accuracy and reliability of the position solution. Furthermore, the integration of additional sensors can be strategically employed to enhance the accuracy and robustness of the 3D positioning system.

4 Conclusion

In this paper, we have demonstrated the potential of mmWave radar sensory technology to be used for accurate cm-level 3D indoor localization. To explore its full capabilities, we have compared mmWave sensor from two vendors (Texas Instruments, Infineon) while we specifically compared the positioning potential of two types of sensors with different degrees of freedom: one that measures distance and azimuth angle to the target (2-DOF) and another one that additionally measures elevation (3-DOF). The measurement precision analysis and experimental positioning results indicate promising capabilities of both systems in achieving high-precision 3D positioning. Using a 2-DOF sensor system we have achieved a 3D positioning accuracy of 17*cm* using a 3D trilateration approach where as with a 3-DOF sensor system we achieved very similar accuracy 16*cm* in a multi-anchor setup with some enhanced robustness and flexibility on its implementation.

Despite this high accuracy, the technology imposes several challenges, difficulties, and limitations when it comes to setting up and using a multi-sensor positioning system. These challenges include sensing limitations of mmWave sensors, the difficulty of detecting stationary targets, the complexity of multi-object detection, and the need for timing synchronization. These challenges were addressed through careful system design and the implementation of appropriate solutions.

5 References

A. Antonucci, M. C. (2019). Performance analysis of a 60-ghz radar for indoor positioning and tracking. *2019 International Conference on Indoor Positioning and Indoor Navigation (IPIN).*

A. Bourdoux; et al. (2020). *6g white paper on localization and sensing*. Retrieved May 2023, from https://arxiv.org/abs/2006.01779

A. Sesyuk, S. I. (n.d.).

A. Sesyuk, S. I. (2022). A survey of 3d indoor localization systems and technologies. *Sensors, 22*(23).

A. Sesyuk, S. I. (2023). 3D millimeter-wave indoor localization. *13th International Conference on Indoor Positioning and Indoor Navigation (IPIN).* Nuremberg.

A. Shahmansoori, G. E.-G. (2018). Position and Orientation Estimation Through Millimeter-Wave MIMO in 5G Systems. *IEEE Transactions on Wireless Communications, 17*(3), 1822-1835.

B. Antonescu, M. T. (2019). Clustering algorithms and validation indices for a wide mmwave spectrum. *Information , 10*(9).

B. Li, K. Z. (2020). Dilution of Precision in Positioning Systems Using Both Angle of Arrival and Time of Arrival Measurements. *IEEE Access, 8*, 192506-192516.

D. Wang, M. F. (2019). Pursuance of mm-Level Accuracy: Ranging and Positioning in mmWave Systems. *IEEE Systems Journal, 13*(2), 1169-1180.

F. Parralejo, J. P. (2023). Mil- limetre wave radar system for safe flight of drones in human-transited environments. *13th International Conference on Indoor Positioning and Indoor Navigation.*

H. He, Y. L. (2021). Clustering algorithm based on azimuth in mmwave massive mimo-noma system. *021 IEEE/CIC International Conference on Communications in China (ICCC Workshops).*

Han, C. &. (2012). Location-aided multi-user beamforming for 60 GHz WPAN systems. 1-5.

Han, Y., Shen, Y., Zhang, X., Win, M. Z., & Meng, H. (n.d.). "Performance Limits and Geometric Properties of Array Localization," in IEEE Transactions on Information Theory, vol. 62, no. 2, pp. 1054-1075, Feb. 2016, doi: 10.1109/TIT.2015.2511778.

Hao, Z., Yan, H., Dang, X., Ma, Z., Jin, P., & Ke, W. (2022). Millimeter-Wave Radar Localization Using Indoor Multipath Effect. *Sensors, 22*(5671).

Hao, Z; et. al. (2022). Millimetre-wave radar localization using indoor multipath effect,. *Sensors, 22*, 5671.

Hunukumbure, O. K. (2022). A drone-based 3d localization solution for emergency services. *ICC 2022 - IEEE International Conference on Communications.*

Laoudias, C., Moreira, A., Kim, S., Lee, S., Wirola, A., & Fischione, C. (2018). A Survey of Enabling Technologies for Network Localization, Tracking, and Navigation. *IEEE Communications Surveys & Tutorials, 20*(4), 3607-3644.

M. T. Moayyed, B. A. (2019). Clustering algorithms and validation indices for mmwave radio multipath propagation. *2019 Wireless Telecommunications Symposium (WTS).*

Maisy Lam, L. D. (2023). 3D Self-Localization of Drones using a Single Millimeter-Wave Anchor. *Robotics*.

Malivert F, L.-I. O. (2023). Comparison and Improvement of 3D-Multilateration for Solving Simultaneous Localization of Drones and UWB Anchors. *Applied Sciences, 13*(2), 1002.

Marques, S. D. (2020). Pursuing drones with drones using millimeter wave radar. *IEEE Robotics and Automation Letters, 5*(3), 4156-4163.

Marrón, C. -Y. (2010). COLA: Complexity-Reduced Trilateration Approach for 3D Localization in Wireless Sensor Networks. *010 Fourth International Conference on Sensor Technologies and Applications.* Venice.

Norrdine, A. (2012). An Algebraic Solution to the Multilateration Problem. *2012 International Conference on Indoor Positioning and Indoor Navigation.*

Ojas Kanhere, T. S. (2018). Position Locationing for Millimeter Wave Systems. *GLOBECOM 2018 - 2018 IEEE Global Communications Conference.*

P. K. Rai, H. I. (2021). Localization and activity classification of unmanned aerial vehicle using mmwave fmcw radars. *IEEE Sensors Journal, 21*(14), 16043-16053.

Saily, M; et. al. (2021). Positioning technology trends and solutions toward 6g. *IEEE 32nd Annual International Symposium on Personal, Indoor and Mobile Radio Communications (PIMRC)*, (pp. 1-7).

Sumathi, V. K. (2012). An efficient clustering algorithm based on z-score ranking method. *2012 International Conference on Computer Communication and Informatics.*

T, W., & al, e. (2021). "Joint design of communication and sensing for beyond 5g and 6g systems. *IEEE Access, 9*(30), 845-857.

Tuo Wu, C. P. (2022). 3D Positioning Algorithm Design for RIS-aided mmWave Systems. *Signal Processing*.

Wang, D., Fattouche, M., & Zhan, X. (2019). Pursuance of mm-Level Accuracy: Ranging and Positioning in mmWave Systems. *IEEE Systems Journal, 13*(2), 1169-1180.

Y. Han, Y. S.-P. (2016). Performance Limits and Geometric Properties of Array Localization. *IEEE Transactions on Information Theory, 62*(2), 1054-1075.

Y. Jia, H. T. (2018). Motion Feature and Millimeter Wave Multi-path AoA-ToA Based 3D Indoor Positioning. *IEEE 29th Annual International Symposium on Personal, Indoor and Mobile Radio Communications (PIMRC).* Bologna .

Yin, Y. C. (2021). Channel Estimation for RIS-aided mmWave Communications via 3D Positioning. *IEEE/CIC International Conference on Communications in China (ICCC Workshops).* Xiamen.

Youqing Wang, K. Z. (22). A 3D Indoor Positioning Method of Wireless Network with Single Base Station in Multipath Environment. *Wireless Communications and Mobile Computing, 2022*.

Yu, S., & Al., e. (2018). A Low-Complexity Autonomous 3D Localization Method for Unmanned Aerial Vehicles by Binocular Stereovision Technology. *10th International Conference on Intelligent Human-Machine Systems and Cybernetics (IHMSC),* , (pp. 344-347).

Z. Lin, T. L. (2018). 3-D Indoor Positioning for Millimeter-Wave Massive MIMO Systems. *IEEE Transactions on Communications, 66*(6), 2472-2486.

Zafari, F., Gkelias, A., & Leung, K. (2019). A Survey of Indoor Localization Systems and Technologies. *IEEE Communications Surveys & Tutorials, 21*(3), 2568-2599.

Zhao, Y., Liang, J. C., Sha, X., & Li, W. (2020). Adaptive 3D Position Estimation of Pedestrians by Wearing One Ankle Sensor. *IEEE Sensors Journa, 20*(19), 11642-11651.